Tissue-resident NK cells support survival in pancreatic cancer through promotion of cDC1-CD8T activity.

Running title

Radiotherapy and CCR5i/αPD1 Immunotherapy induce trNK cells and PDAC tumor control.

Authors

Simei Go[1], Constantinos Demetriou[1], Sophie Hughes[1], Simone Lanfredini[1], Giampiero Valenzano[1], Helen Ferry[2], Edward Arbe-Barnes[3], Shivan Sivakumar[1], Rachael Bashford-Rogers[4], Mark R. Middleton[1,2,5], Somnath Mukherjee[5], Jennifer Morton[6,7], Keaton Jones[8], Eric O'Neill[1]

Affiliations

[1]Department of Oncology, University of Oxford; Oxford, UK

[2]NIHR Oxford Biomedical Research Centre, Oxford University Hospitals.

[3]University of Oxford Medical School, OX3 9DU Oxford, UK

[4]Department of Biochemistry, University of Oxford, OX1 3QU Oxford, UK

[5]Oxford University Hospitals NHS Foundation Trust, Oxford, UK

[6]CRUK Beatson Institute, Garscube Estate, Switchback Road, Glasgow, G61 1BD, UK

[7]School of Cancer Sciences, University of Glasgow, Garscube Estate, Glasgow, G61 1QH, UK

[8]Nuffield Department of Surgical Sciences, University of Oxford; Oxford, UK

Contact information

Eric O'Neill

Department of Oncology

University of Oxford

Old Road Campus Research Building

Roosevelt Drive

Oxford

OX3 7DQ

eric.oneill@oncology.ox.ac.uk

Abstract

The immunosuppressive microenvironment in PDAC prevents tumor control but strategies to restore anti-cancer immunology, by increasing CD8 T cell activity, have not been successful. Here we demonstrate how inducing localized physical damage using ionizing radiation (IR) unmasks the benefit of immunotherapy by increasing tissue-resident NK (trNK) cells that support CD8 T activity. Our data confirms that targeting mouse orthotopic PDAC tumors with IR together with CCR5 inhibition and PD1 blockade reduces E-cadherin positive tumor cells by recruiting a hypofunctional NKG2C^{-ve} NK population that supports CD8 T cell involvement. We show an equivalent population in human PDAC cohorts that represents an adaptive-like immunomodulatory trNK-cell that similarly supports CD8 T cell levels in a cDC1-dependent manner. Importantly, a trNK signature associates with survival in PDAC and solid malignancies revealing a potential beneficial role for trNK in improving adaptive anti-tumor responses and supporting CCR5i/αPD1 and IR-induced damage as a novel therapeutic approach.

Introduction

Over the past decade, immune checkpoint inhibitors have shown significant success in the treatment of various solid malignancies. Treatment of pancreatic cancer using immunotherapy alone or in combination with radiotherapy or chemotherapy has unfortunately seen limited clinical success over either modality alone(Bockorny et al., 2020; Doi et al., 2019; Royal et al., 2010; Weiss et al., 2018; Weiss et al., 2017) (Mohindra et al., 2015). This is likely due to several tumor microenvironmental factors, including the dense stroma that supports an immunosuppressive environment while also obstructing the infiltration of cytotoxic immune cells(Mills et al., 2022; Piper et al., 2023). Novel strategies comprising dual targeting of PD-1/IL-2Rβγ with radiotherapy are beginning to indicate that potential benefits may require a coordinated alteration in the suppressive microenvironment involving loss of regulatory T cells (Tregs) and increased natural killer (NK) cell infiltration, in addition to simply increasing CD8 T infiltration(Piper et al., 2023).

We previously identified serum CCL5 as a negative prognostic marker for late-stage advanced pancreatic cancer(Willenbrock et al., 2021). CCL5 (RANTES) is pro-inflammatory and an acute response to injury or infection that promotes recruitment of monocytes and lymphoid immune cells through CCR5, CCR3, and CCR1. In cancer, sustained CCL5-mediated inflammation leads to a suppressive environment via attraction of $CCR5^+$ immunoregulatory components, including Tregs, tumor-associated macrophages (TAMs), and myeloid-derived suppressor cells (MDSCs) normally involved in resolving inflammatory events (Hemmatazad and Berger, 2021). Pancreatic tumors that are poorly differentiated produce higher levels of CCL5 and express more of its main receptor, CCR5, compared to well-differentiated and non-cancerous tissue(Monti et al., 2004; Singh et al., 2018). Disrupting this loop by the FDA-approved CCR5 inhibitor maraviroc reduces pancreatic tumor cell migration, invasiveness(Singh et al., 2018) and proliferation(Huang et al., 2020). Silencing CCL5 expression in Panc02 cells or systemic administration of the CCR5 inhibitor TAK-779 reduces Treg migration and tumor volume in a murine subcutaneous tumor model(Tan et al., 2009). These studies suggest that the CCL5/CCR5 axis may be a promising therapeutic target in pancreatic cancer as it has the potential to alter both the intrinsic properties of tumor cells and immune cell migration.

In established pancreatic tumors, the immune suppressive environment promotes more tissue repair/resolution signaling (M2-like macrophages, MDSCs) and prevents pro-inflammatory signaling (M1-like macrophages). Radiotherapy is delivered to localized tumors to stimulate a pro-inflammatory environment and increase the opportunity for tumor neo-antigens to be recognized by infiltrating adaptive response cells. As such, stereotactic ablative radiotherapy (SBRT) delivers high doses of radiotherapy in a minimal number of fractions to maximize an inflammatory cascade but the sensitivity of lymphocytes to DNA damage and the immune suppressive environment prevent benefit

79 or meaningful tumor control(Mills et al., 2022). In NSCLC, single cell RNA sequencing (scSeq) of
80 immune cells within tumors identifies a distinct subset of CD49a$^+$ CD103$^+$ tissue-resident memory
81 (TRM) CD8$^+$ T cells that have capacity to respond to neo-antigens but are suppressed(Caushi et al.,
82 2021). In this case, the use of an anti-PD1 antibody (αPD1) supports TRM activation but additional
83 disruption of the immune suppressive environment is still required, indicating that additional
84 components are required in addition to simply activating CD8$^+$ T cell neo-antigen recognition.
85 Kirchhammer et al. recently reported that a tissue-resident NK (trNK) cell population is induced in
86 NSCLC in response to viral delivery of IL-12, which crucially supported type I conventional dendritic
87 cell (cDC1) infiltration and increased DC-CD8$^+$ T cell interactions(Kirchhammer et al., 2022). Together
88 with PD1 blockade, IL-12-mediated recruitment of trNK cells enhances cross-presentation of antigen
89 to CD8 T via cDC1 suggesting this represents a substantial barrier for T cell focused therapy and that
90 improving the NK/DC/T-cell crosstalk can promote antitumor immunity and tumor control. Notably,
91 this was dependent on CCL5 and points to a positive role for inflammatory CCL5 signaling in the
92 absence of CCR5-mediated suppression(Kirchhammer et al., 2022).
93 Given the negative prognosis associated with high CCL5 serum levels in human patients and
94 its diverse functions in chemokine and paracrine signaling (Aldinucci et al., 2020), we hypothesized
95 that inhibiting CCR5 rather than CCL5, in combination with radiotherapy and anti-PD1
96 immunotherapy may improve tumor control via a multimodal approach. To test this, we employed a
97 murine orthotopic pancreatic cancer model and monitored tumor growth and immune infiltration.
98 We find that while the use of a CCR5 inhibitor (CCR5i) alone restricts Treg involvement, it does not
99 impact tumor viability alone or together with αPD1. However, in combination with radiotherapy, we
100 see a significant alteration in MDSCs, NK and CD8 T cells and better tumor control. Interestingly, we
101 observe that IR/CCR5i/αPD1 combination treatment induced a trNK population that is the highly
102 correlated immune population with tumor control. Exploration of scRNA-seq datasets from human
103 PDAC studies confirms the presence of trNK cells as immunomodulatory in human PDAC, and directly
104 supports cDC1-CD8 communication. Strikingly, a specific trNK signature indicates that higher levels of
105 this NK subtype are significantly correlated with better PDAC patient overall and disease-free survival.
106 Moreover, pan-cancer analysis reveals trNK cell involvement is associated with better patient survival
107 across a number of solid tumors and supports the potential utility of a combination regimen
108 comprising ionizing radiation (IR) and CCR5i/αPD1 immunotherapy (IO) as a promising strategy to
109 increase NK/cDC1/CD8 mediated tumor control in solid cancers.

110 ## Results

111 ### CCL5 is a negative prognostic marker in pancreatic cancer

112 We previously identified serum CCL5 as a *bona fide* negative prognostic marker for pancreatic
113 cancer(Willenbrock et al., 2021), and found that, in two independent PDAC cohorts
114 (CPTAC3(Cao et al., 2021) and TCGA(Uhlen et al., 2017)), higher CCL5 expression associates
115 with poor overall and disease-free survival, confirming the negative implication of high levels
116 of CCL5 in pancreatic cancer (Figure 1A). To understand the cause of CCL5-mediated reduced
117 survival in PDAC, we hypothesized that immune cells responsive to a CCL5 chemotactic
118 gradient (through expression of the cognate receptors CCR5, CCR3 or CCR1) could be
119 potential contributors to an adverse tumor immune environment (Figure 1B, figure
120 supplement 1A). Single cell sequencing of human tumors has revealed genetic signatures for
121 myeloid derived suppressor cells of polymorphonuclear (PMN-MDSC) or monocytic (M-
122 MDSC) origin(Alshetaiwi et al., 2020), TAMs(Wang et al., 2021), CD4 T-regulatory cells
123 (Treg)(Mijnheer et al., 2021) and NK cells(Smith et al., 2020), but none of these immune
124 populations have yet been implicated as a causative agent in the poor outcome associated
125 with high CCL5 expression in PDAC (Figure 1C). Notably, exploration of individual genes
126 within these signatures indicated stark opposing correlations within each signature pool –
127 particularly for genes associated with MDSCs (S100P vs ARG2) and NK cells (CD56 vs CD16)
128 (Figure 1C, figure supplement 1B). CD56 (*NCAM1*) is a key marker that represents functionally
129 distinct subpopulations of NK cells where $CD56^{bright}$ NK cells represent naïve states that move
130 to $CD56^{dim}$ upon maturation to full cytotoxic potential, whereas conversely $CD16^{+}$ expression
131 marks activation and $CD16^{-}$ immature or quiescent NK cells(Poli et al., 2009). Thus, these
132 distinct subtypes may differentially contribute to survival, e.g., association of CD16 with poor
133 survival may implicate a detrimental role of $CD56^{dim}CD16^{+}$ NK cells, whereas the strong
134 positive prognosis associated with CD56 expression could indicate benefit of $CD56^{bright}CD16^{-}$
135 NK cells. The benefit of CD56 can be attributed to NK cells over neuronal expression as the
136 neuronal-cell specific homolog *NCAM2* has no prognostic value (figure supplement 1C).

137 ### CCR5i modulates Treg infiltration in an orthotopic pancreatic tumor model

138 We next employed a syngeneic orthotopic pancreatic cancer model where cells derived from
139 *Kras*^{G12D}, *Trp53*^{R172H}, *Pdx1-Cre* C56/BL6 tumor bearing mice are injected into the pancreas of
140 wildtype C56/BL6 mice recapitulating a human pancreatic cancer microenvironment(Matzke-

141 Ogi et al., 2016). From a selection of independently isolated KPC derived cell lines, we first
142 determined the cell line KPC_F as an appropriate model for human PDAC tumor based on
143 expression of epithelial (E-cadherin), mesenchymal (vimentin), stromal (Collagen I, αSMA)
144 markers as well as displaying both growth kinetics (determined by MRI) amenable for the
145 study and expression of high levels of CCL5 (Figure 2A, figure supplement 2A/B). To address
146 which immune subsets are involved in CCL5 signaling in pancreatic cancer, we developed a
147 17-color spectral flow cytometry panel to monitor the tumor-infiltrating immune
148 microenvironment in parallel, (figure supplement 2C) and employed a specific CCR5 inhibitor
149 (Maraviroc, CCR5i), to block CCR5, the most widespread and highest-affinity receptor for
150 CCL5 expressed on Tregs (figure supplement 1A).

151 Pilot experiments injecting 500 KPC-F cells yielded robust and replicative growth
152 kinetics (indicated by matching volumes of ±100 mm^3 at the beginning of exponential
153 growth), permitting direct comparisons of infiltrating immune cells across different treatment
154 groups (Figure 2A). Next, tumors were allowed to reach 50 mm^3 (approx. 12 days) before
155 initiation of treatment with daily CCR5i for 7 days. Mice were culled 30 days post-treatment
156 for the characterization of infiltrating immune cells (Figure 2B). Notably, CCR5i significantly
157 reduced Treg infiltration but had no effect on the infiltration of other immune cells,
158 indicating the active recruitment of $CCR5^+$ Tregs in PDAC (Figure 2B). Given the limited effect
159 of CCR5i on tumor growth kinetics and immune infiltration, however, standalone inhibition of
160 CCR5 and the resultant lack of recruitment of Tregs alone are unlikely to impact PDAC
161 progression.

162 Combination immunotherapy following localized damage alters tumor of immune composition

163 Induction of a localized inflammatory microenvironment with ionising radiation (IR) can drive
164 anti-tumor responses, but radiotherapy has had limited success in treatment of PDAC and
165 combination with immune checkpoint inhibitors (e.g. αPD1) does not increase benefit.
166 Therefore, we next examined whether the addition of CCR5i to tumor-targeted IR could
167 overcome this by further modulating immune cell migration, in particular by reducing Treg
168 involvement (Figure 3A, figure supplement 3A). As expected, radiotherapy (3 x 4Gy)
169 produced a strong effect on gross tumor volume, significantly reducing volumes over
170 standalone treatment with αPD1, CCR5i or CCR5i+αPD1 (Figure 3A). Responses to
171 combination of IR with CCR5i, αPD1 or CCR5i+αPD1 (IR+IT) showed larger variations

172 compared to IR alone, implying mixtures of 'responders' and 'non-responders' to immune-
173 modulatory treatments. Moreover, IR/CCR5i/αPD1 treated tumor sections had significantly
174 reduced DAPI$^+$ and p53$^+$ KPC cells compared to all other conditions, suggesting significantly
175 more loss of tumor cells by triple combination treatment (Figure 3B, figure supplement 3B-C).
176 Tumor sections from the triple combination treatment also presented with increased loss of
177 active stroma (αSMA staining, figure supplement 3D) and increased necrotic areas over
178 standalone radiotherapy (Figure 3C). In line with apparent increased tumor control, the triple
179 combination treatment demonstrated infiltration of CD8$^+$ T cells (Figure 3D), supporting
180 greater penetration of CD8$^+$ T cells into the centre of tumors (figure supplement 3E). These
181 results support improved tumor control with combination of IR+CCR5i+αPD1 over standalone
182 radiotherapy or IR in combination with αPD1 and CCR5i alone. To elucidate the immune
183 mechanisms behind this control, we analysed the immune infiltrate of pancreatic tumors. In
184 line with the results above, the triple combination reduced Treg infiltration, enhanced CD8$^+$ T
185 cell infiltration and supported a moderate increase in CD4$^+$ T helper cells (Figure 3E, figure
186 supplement 3F).

187 Interestingly, no alteration was seen in the myeloid compartment, except for a
188 reduced infiltration of PMN-MDSCs, whereas a significant infiltration of NK and NKT cells
189 could be observed in pairwise comparisons between IR+αPD1 vs IR+CCR5i or IR+CCR5i+αPD1
190 (Figure 3E, figure supplement 3F). These results collectively support the notion that
191 IR/CCR5i/αPD1 combination treatment alters immune infiltration by reducing Tregs and
192 increasing NK and CD8 T cells, thereby resulting in greater local tumor control.

193 CD8 and NKG2D$^-$ NK cells correlate with increased tumor control

194 To derive more granularity on the potential roles of NK- and T-cell populations in tumor
195 control, tissue sections were stained using an optimized multiplex immunofluorescence panel
196 and analyzed by HALO AI software to identify tumor cells (E-cadherin$^+$ - blue), CD8$^+$ T cells
197 (CD3$^+$CD8$^+$ - orange), CD4$^+$ T-cells (CD3$^+$CD8$^-$ - green) and NK cells (CD3$^-$CD8$^-$NK1.1$^+$ - red)
198 (Figure 4A, figure supplement 4A). As observed with flow cytometric and
199 immunohistochemical analyses, multiplex staining of tumor sections also revealed a
200 significant increase of CD8$^+$ T cells per mm^3 when IR was used in combination with CCR5i or
201 CCR5i/αPD1 (figure supplement 4B). Notably, despite having responders and non-responders
202 in the combination groups (Figure 4A), a significant overall reduction in E-cadherin$^+$ tumor

203 cells as a percentage of total DAPI$^+$ cells was observed (Figure 4B), supporting a decrease in
204 cellularity and an increase in tumor necrosis with the IR/CCR5i/αPD1 combination (Figure
205 3B,C). The increase in CD8$^+$ T cells with combination treatment appears independent of
206 tumor area and is matched by a similar increase in NK cells (Figure 4B, figure supplement 4B).
207 To correlate immune infiltration against loss of tumor cells (a measure of local tumor control)
208 we determined relationships between CD4 T, CD8 T and NK cell populations and E-cadherin$^+$
209 cells across all tumor sections (independent of treatment) and found a significant inverse
210 correlation for both CD8 T and NK cells (r^2=-0.3, p=0.038 and r^2=-0.33, p=0.026 respectively),
211 but not CD4 T cells (Figure 4C).

212 We next checked if the association between NK cells and loss of tumor cells was due
213 to killing by functionally active NK cells by focusing our analysis on the NKG2D$^+$ NK cell
214 population, given that this is one of the major activating receptors on NK cells and is required
215 for the lysis of target cells(Bryceson and Ljunggren, 2008). Surprisingly, the proportion of
216 infiltrating CD3$^-$CD161$^+$NKG2D$^+$ cells (NK^{Active}) is reduced under IR/CCR5i/αPD1 combination
217 treatment, implying a decrease in total NK cell cytolytic capacity (figure supplement 4C). The
218 reduced NKG2D expression on NK cells may be a result of the prolonged engagement by
219 ligands expressed on tumor cells, followed by ligand-induced endocytosis and
220 degradation(Quatrini et al., 2015), or the shedding of NKG2D ligands by tumor cells(Kaiser et
221 al., 2007). In both instances, receptor down-regulation causes a reduction in cytotoxicity and
222 impairs NK cell responsiveness to tumor cells, potentially contributing to exhaustion(Groh et
223 al., 2002). Not surprisingly, the reciprocal CD3$^-$CD161$^+$NKG2D$^-$ population increases upon
224 triple combination treatment (figure supplement 4C). Interestingly, circulating NK cells from
225 PDAC patients show reduced NKG2D levels compared to healthy controls(Peng et al., 2013)
226 supporting the notion that chronic exposure to NKG2D ligands expressed or shed by PDAC
227 cells might cause NKG2D down-modulation and a hyporesponsive phenotype. Surprisingly,
228 the correlation of NK cells with decreased frequency of E-cadherin$^+$ cells was completely
229 abrogated with selection for more functionally competent NK cells (NK^{Active}), implying the
230 opposite hypofunctional NKG2D$^-$ NK population (NK$^{NKG2D\text{-}ve}$) is responsible for correlation of
231 NK cells with E-cadherin loss and indeed, a superior inverse correlation is observed for
232 NK$^{NKG2D\text{-}ve}$ and Ecadherin compared to NK^{Active} or NK^{Total} (r^2=-0.52, p=0.003) (Figure 4D). To
233 explore this association is relation to tumor control, sections were split into either E-
234 cadherin^{high} or E-cadherin^{low} and the extent of immune involvement was represented as a

235 percentage of total DAPI^{+}. While CD8 T cells significantly segregated with E-cadherin^{low},
236 implying a contribution to tumor control, the association of NK$^{NKG2D-ve}$ was vastly more
237 significant (Figure 4E).

238 **Heterogenous subsets of NK cells in PDAC exhibit differential inhibitory and activatory signatures**

239 To extrapolate our findings to the human setting, we explored scRNA-seq data from selected
240 NK and T-cells derived from human pancreatic cancer patients. A total of 51,561 cells were
241 catalogued into 17 distinct cell lineages annotated with canonical gene signatures as
242 described in Steele *et al.* using unsupervised clustering(Steele et al., 2020) (figure supplement
243 5A). UMAP projection of the lymphocyte compartment does not delineate NK subpopulations
244 and shows overlap with CD8 T cells (figure supplement 5B). Therefore, we focused on UMAP
245 projections of the CD8 and NK compartment alone to reveal three clear NK subpopulations
246 that are distinct from CD8 T cells and clearly separate out in clusters of immature (NK_C3),
247 active (NK_C2) and reduced activation (NK_C1) NK cells from T cells (Figure 5A). In agreement
248 with downregulation of circulating NKG2D^{+} in PDAC patients, NKG2D (KLRK1) expression was
249 below detection across all CD8 and NK subpopulations retrieved from patient tumors(Groh et
250 al., 2002). As expected, CD16^{high} (FCGR3a) cytotoxic NK cells (NK_C3) cluster separately from
251 CD16^{-} NK cells (NK_C1) which are more enriched for genes related to cytokine secretion than
252 cytolytic function (Figure 5D, figure supplement 5C). The NK_C1 cluster correlates best with
253 the hypofunction NK phenotype observed in mice as similarly displayed reduced activation
254 (reduced NKG7, NKp80, GZMA and PRF1) with additional expression of tissue residency
255 markers *CD103*, *CD49a* and, surprisingly, the adaptive activating receptor NKG2C (*KLRC2*)
256 (Figure 5B, C). While adaptive-like NK cells in circulating are associated with a Cd56^{dim}CD16^{+}
257 phenotype, adaptive like (i.e. NKG2C^{+}) tissue resident NK cells have been identified in lung
258 tissue(Brownlie et al., 2021) and appear to match our pancreatic tissue NK_C1 cells.
259 Downstream UMAP analysis of the NK cell population distinguishes these 3 subsets of NK
260 cells (NK_C1, NK_C2 and NK_C3) based on 41 differentially expressed genes (Figure 5D, E).

261 Given that CD56 expression correlates with increased survival in PDAC patients
262 (Figure 1C) we were intrigued to notice that the hypofunctional NK_C1 cluster is enriched for
263 CD56 but not CD16 expression (Figure 5D). These data suggest that NK_C1 cluster represents
264 a subset of NK cells in PDAC that display tissue-residency markers (*ITGAE,* CD103 and *ITGA1,*
265 CD49a) and have an immune-secretory phenotype (XCL1) as opposed to cytolytic phenotype

266 (NK_C2 CD16$^+$, NKG7$^+$) (Figure 5E). Furthermore, we define a core signature gene set to
267 distinguish NK_C1 from other NK subpopulations (Figure 5F). Verification of the NK_C1
268 population as NKG2C$^+$ and tissue resident (trNK) in a second scRNA pancreatic cancer dataset
269 of Peng *et al.*(Peng et al., 2013) confirmed the existence of these cells in an independent
270 PDAC cohort, again hypofunctional for cytotoxic activity and enriched for the inhibitory
271 receptor NKG2A (KLRC1) (figure supplement 5D, E, F).

272 Tissue resident NK cells in PDAC show differential communication

273 The NK_C1 population had the highest expression of the chemokines XCL1 and XCL2, which
274 have been demonstrated to attract type-1 conventional dendritic cells (cDC1)(Böttcher et al.,
275 2018) and thereby increase cross presentation to CD8$^+$ T cells. We next explored myeloid
276 populations in the Steele *et al.* scPDAC dataset (figure supplement 6A) and identified cDC1
277 cells as XCR1$^+$ enriched compared to other DC subsets (Figure 6A, figure supplement 6B). As
278 XCR1 is the receptor for XCL1/2, this suggests that a main direction of communication is from
279 NK_C1 cells in PDAC is to cDC1 (Figure 6B). We next employed the R-package 'CellChat'(Jin et
280 al., 2021) to further dissect the crosstalk between NK_C1 and other cells found in the
281 pancreatic tumor microenvironment, and confirmed NK_C1-derived XCL1/2 is the strongest
282 signal to XCR1$^+$ cDC1s (Figure 6C). Analysis of specific ligand-receptor pairs between NK_C1
283 and 24 other cell groups yielded 32 significant interactions, of which the TNFSF14 (LIGHT)-
284 TNFRSF14 pair was the most universal intercellular interaction, whereas CD74 (or MIF)
285 signaling showed the highest communication probability (figure supplement 6C).

286 Within the immune cell compartment, communication signals between NK_C1 and
287 macrophages were the most abundant and diverse, followed by cDCs (cDC2 and cDC1) and
288 Tregs (figure supplement 6C). Similarly, cDC1 from in these PDAC samples capable of
289 presenting MHC class I peptides to CD8$^+$ T cells, but surprisingly also MHC class II to CD4$^+$
290 Tregs (figure supplement 6D). Next, significant receptor-ligand interactions were segregated
291 as 'outgoing' or 'incoming' signals to understand directionality of communication. Among the
292 outgoing signals from different cell types, NK_C1 cells contributed the highest IL-16, CSF,
293 LIGHT (TNFSF14), FASLG and MIF signals in tumors (Figure 6D). IL-16 is mainly known as a
294 chemoattractant for CD4$^+$ T cells, however CD4$^+$ dendritic cells exist and have also been
295 demonstrated to be recruited by IL-16 (Bialecki et al., 2011; Kaser et al., 1999; Vremec et al.,
296 2000). IL-16 has also been described to increase HLA-DR levels in CD4$^+$ T cells and

297 eosinophils, therefore has the potential to induce MHC antigen presentation in $CD4^+$
298 cells(Cruikshank et al., 1987; Rand et al., 1991). Taken together, these interactions support
299 the hypothesis that trNK cells may improve tumor control via recruitment of type 1 dendritic
300 cells via XCR1, while promoting DC maturation via LIGHT-CD86(Zou and Hu, 2005) signaling
301 and supporting antigen presentation to both $CD4^+$ and $CD8^+$ T cells via MIF-CD74 signaling
302 (Basha et al., 2012) (Figure 6E). On the other hand, dendritic cell-secreted BAG6 may
303 promote both survival and cytokine release by NK cells by binding NKp30(Simhadri et al.,
304 2008) and directly signal to CD8 T cells via CXCL16-CXCR6(Di Pilato et al., 2021), thereby
305 generating an anti-tumor feedforward loop (Figure 6E). Remarkably, IL-16 also communicates
306 to $CD4^+$ Tregs and $CD74^+$ fibroblasts, likely supporting tumor growth (Figure 6D). However,
307 both cell types may be susceptible to Fas-mediated cell death due to NK_C1 expression of Fas
308 ligand (Figure 6D). This could enhance immune cell infiltration and revoke the
309 immunosuppressive environment, ultimately contributing to increased tumor control.

310 These results so far suggest the presence of immunoregulatory trNK cells in PDAC that
311 are involved in an intricate immune communication network with DCs and CD8 T cells to
312 enhance anti-tumor immunity. To support this hypothesis, we explored the correlation
313 between trNK and CD8 T infiltration in our KPC_F orthotopic tumor model and found a highly
314 significant positive association (R^2 = 0.6571, p = 0.003) which was strengthened when we
315 focused on untreated (Mock) versus IR+IT combinations where trNK cells are evident (R^2 =
316 0.9223, p = 0.0004) (Figure 6F). To ascertain if this also holds true in human PDAC, we first
317 specified the NK_C1 signature as a 14-gene signature that was specific for our tissue-resident
318 NK cells over all other cells to distinguish levels in bulk datasets (Table 1). We next explored
319 the CD8 T:trNK cell relationship in PAAD_TCGA and, as the model in Figure 6E predicts this
320 interaction to be cDC1 dependent, by binning PAAD_TCGA cohort into quartiles based
321 differential cDC1 signature expression to test dependence of CD8 T:trNK on cDC1 levels
322 (Figure 6G). PDAC patient tumors with the lowest evidence for cDC1 involvement have a
323 weak correlation of trNK_C1 with CD8A and CD8B (p = 0.047; p = 0.45 respectively) which
324 rises to a strong highly significant correlation when the highest levels of cDC1s are present
325 (R^2 0.3, trNK_C1 vs CD8A p = 0.0001; R^2 0.34, trNK_C1 vs CD8B p = 0.000047) (Figure 6G).

326 NK cell signature correlates with improved survival

327 As the presence of trNK and correlation with CD8 T cells appears boosted by IR, we next
328 explored our original finding that CD56 correlates with highly significant survival in PDAC
329 (Figure 1, figure supplement 1). We hypothesized that tumors with a high *CD56* signature
330 might recruit a high proportion of trNK ($CD56^{bright}CD16^{low}$), whereas tumors with a low CD56
331 signature might have a lower proportion of trNK and, therefore, could benefit from IR.
332 Indeed, separating PAAD_TCGA patients into those who received radiotherapy (RTx) versus
333 those that did not, showed that the benefit in overall survival of PDAC patients is only
334 apparent in the $CD56^{low}$ patient group (log rank $p < 0.0001$, Figure 7A). We next explored
335 whether CD56-associated survival is specifically due to the presence of trNK cells using our
336 NK_C1 signature (Table 1). Analysis of primary PDAC tumors from the TCGA (TCGA_PAAD)
337 demonstrates that patients with tumors enriched for the trNK cell (NK_C1) gene signature
338 were associated with improved PDAC survival compared to patients without trNK
339 involvement (Figure 7B, figure supplement 7A). Similarly to $CD56^{low}$ patients, we find that
340 patients with $trNK^{low}$ benefit from RTx (log rank $p < 0.005$, Figure 7C). Notably, we find that
341 despite an overall poor prognosis, $CCL5^{high}$ patients (TCGA and CPTAC3) are significantly
342 enriched for the trNK_C1 gene signature (Figure 7D), potentially due to strong CCR5 or CCR1-
343 mediated recruitment (figure supplement 1A). However, as CCL5 also recruits MDSCs, TAMs,
344 Tregs and conventional NK cells via CCR5, CCR5i prevents a tumor suppressive
345 microenvironment, both directly and indirectly by retaining trNK cells that remove Tregs
346 through FASL (figure supplement 7B). Therefore, we could expect that patients with $CCL5^{high}$
347 NK_C1^{low} would perform significantly worse than patients with $CCL5^{high}NK_C1^{high}$. Indeed,
348 $CCL5^{high}$ patients enriched for the NK_C1 signature or CD56 had significantly improved overall
349 and disease-free survival (Figure 7E, F). This also supports a model where CCL5 mediated
350 recruitment of NK cells can be beneficial in the absence of CCL5-CCR5 recruitment, via
351 CCR1(Ajuebor et al., 2007) (figure supplement 7C, 1A). These results suggest that despite
352 high CCL5 levels and an overall poor prognostic outcome, the presence of tissue-resident NK
353 cells significantly improves survival and provides an opportunity for intervention with the
354 IR+IT combination.

355 Finally, we explored whether the NK_C1 gene signature could be a prognostic marker
356 in solid malignancies other than PDAC by expanding our TCGA analysis. The majority of
357 cancers with enriched expression of our NK_C1 gene signature showed improved survival
358 apart from endometrium and prostate (Figure 8), as a continuous variable or as a high vs low

359 in a univariate Cox regression (figure supplement 8A,B). The latter result confirms our
360 hypothesis that enrichment of trNK cells is a protective factor across most solid malignancies.
361 Moreover, the ability to enrich for this population with IR/IO combinatorial strategies
362 supports the idea that trNK cells generally improve overall survival though improving CD8 T
363 cell activity in solid cancers.
364

365 ## Discussion

366 Novel approaches such as immunotherapies struggle to improve outcome in PDAC as tumors
367 are stromal rich, myeloid-involved immunosuppressive microenvironments devoid of
368 cytotoxic lymphocytes. Most strategies to combat immune suppression, e.g. targeting
369 inhibitory checkpoints such as PD1/PDL1, fail as single therapies because PDAC is largely
370 devoid of the CD8 T cells these agents are designed to reactivate. Combining them with
371 inhibitors of myeloid suppression (e.g. CXCR2) to increase CD8 T penetration also failed to
372 impact survival in clinical trials despite showing promise in pre-clinical studies(Steele et al.,
373 2015),(Siolas et al., 2020). Similarly, high-dose hypo-fractionated ablative radiotherapy has
374 been employed to create an acute localized inflammatory response to stimulate intra-
375 tumoral penetration of CD8 T cells, but even in conjunction with PD1/PDL1 blockade this
376 approach has not shown benefit in PDAC(Parikh et al., 2021). Novel strategies in pre-clinical
377 PDAC models comprising ionizing radiation (IR), αPD1 and BMS-687681 (a dual CCR2/CCR5
378 inhibitor) have shown promising increases in CD8 T cells(Wang et al., 2022) whereas the
379 combination of IR and the bifunctional agent αPD-1/IL-2Rβγ stimulates tumor penetration of
380 polyfunctional stem-like activated CD8 T cells and DNAM1^{+} cytotoxic natural killer (NK)
381 cells(Piper et al., 2023). Together, these approaches indicate potential benefits of a
382 coordinated alteration of the suppressive microenvironment and checkpoint blockade to
383 reduce regulatory T cells (Tregs) and increase NK cell infiltration in addition to supporting
384 CD8 T cell activity. The utility of RT for localized PDAC has been controversial but innovative
385 technology can now deliver ionizing radiation at higher-doses with greater precision(Mills et
386 al., 2022). Rather than simple ablative radiotherapy, this strategy is being employ to increase
387 localized damage that stimulates an acute damage response in immune-cold tumors or
388 increase tumor neoantigens to stimulate adaptive responses(Sodergren et al., 2020). In
389 support of this, the use of IR alongside αPD-1/IL-2Rβγ or FAKi appeared to induce durable
390 immunity in preclinical models(Lander et al., 2022; Piper et al., 2023), suggesting the
391 induction of immunologic memory against tumor antigens is possible.

392 We were led by our previous clinical trial results implicating serum CCL5 levels as a negative
393 prognostic marker for PDAC survival, which we now validate in two independent validation
394 datasets. CCL5 has both pro-inflammatory roles as a chemoattractant for leukocytes and anti-
395 inflammatory activity via recruitment of CCR5^{+} Tregs(Tan et al., 2009). To maintain beneficial

396 signals but limit pro-tumorigenic signaling, we targeted CCR5 alone using maraviroc. Not
397 surprisingly, in an orthotopic KPC model of PDAC we found that Tregs were restricted by
398 CCR5i directly, and the combination of IR and immunotherapy+(IT, CCR5i, αPD1 or
399 CCR5i/αPD1) correlates with a progressive enrichment of CD8 T cells. Intriguingly, CD8 T cells
400 alone were insufficient to explain the loss of cellularity or the increase in necrotic tumors
401 seen with the IR/CCR5i/αPD1 combination, but we do observe a significant increase in total
402 NK and NKT cells that correlates with better local control.
403 NK infiltration has been associated with positive outcomes in many solid tumors, considered
404 to be due to the positive impact of cytotoxic NK cells in cytotoxic CD8 T-mediated tumor
405 clearance(Nersesian et al., 2021). However, the data supporting the independent
406 contribution of NK activity is difficult to discern due to overlap of expression profiles of
407 cytotoxic cells. Surprisingly, markers of cytotoxic cells or specific CD8/CD4 lymphocyte
408 receptors do not perform as indicators of survival from bulk mRNA datasets (Figure 5). This
409 may be due to sensitivity issues but, more likely, the presence of cytotoxic cells alone does
410 not necessarily indicate beneficial responses in patients(Nersesian et al., 2021). This is
411 supported by the limited efficacy of immunotherapy strategies to tumors with a high
412 mutational burden. NK cells represent a variety of subsets defined by surface markers, found
413 in the periphery (circulating), secondary lymphoid organs (spleen, lymph nodes), and specific
414 tissues (e.g. lung, liver, uterus) where markers of tissue residency increase retention or
415 prevent egress(Hashemi and Malarkannan, 2020). In addition to tissue-resident NK cells,
416 tumors appear to accumulate NK populations that become less cytotoxic through
417 downregulation of activating receptors, (NKG2D, NKp40, NKp44) and increased expression of
418 inhibitory receptors (NKG2A) or repression/exhaustion markers (e.g. TIGIT, TIM3) (Hashemi
419 and Malarkannan, 2020) (Marcon et al., 2020). Importantly, NK tissue-resident or
420 hypoactivated subsets commonly display a reduction in cytotoxicity but become highly active
421 immunomodulatory players via expression of XCL1 and XCL2(de Andrade et al., 2019). In
422 melanoma, NK-mediated expression of XCL1 is crucial for the migration of $XCR1^{+}$
423 conventional type 1 dendritic cells (cDC1) and therefore the non-cytotoxic NK subsets in
424 tumors may be vital for cDC1-mediated cross-presentation of tumor antigens to CD 8 T
425 cells(Böttcher et al., 2018). This may explain why levels of CD8 T cells in tumors or removal of
426 inhibitory signaling is insufficient to gain tumor control. Thus, therapeutic strategies aimed at

427 increasing the presence of cDC1 or NK cells may work in combination to support treatments
428 that induce CD8 T cell activity.
429 Our data suggest that combination therapy to stimulate an acute inflammatory response (IR)
430 together with CCR5i/αPD1 (IT) sufficiently modulates the tumor immune microenvironment
431 to improve tumor control. As frequently observed in solid tumors, reduction of cancer cells
432 correlates with intra-tumoral infiltration of NK cells ($CD56^{bright}CD16^{-}$) and improved CD8 T cell
433 penetration(Wu et al., 2020). Surprisingly, our tumors were penetrated by $NKG2D^{-}$ NK cells,
434 suggesting a population with reduced cytotoxicity (figure supplement 5C) which we
435 correlated to a similar population (NK_C1) identified from scRNAseq of human PDAC
436 samples. This population was $CD56^{+}CD16^{-}NKG2C^{+}$, in keeping with adaptive-like tissue
437 resident NK cells(Brownlie et al., 2021; Ruckert et al., 2022) and the apparent beneficial
438 association of CD56 expression with PDAC survival we identified above. NKG2C is a marker of
439 adaptive-like NK cells during viral infections where they offer a potential memory capability
440 to innate immunity(Brownlie et al., 2021; Lopez-Botet et al., 2023). First identified as a
441 subpopulation of blood derived $CD16^{+}$ NK cells in response to viral infection but more
442 recently found to be independent of CD16 expression in tissue (Brownlie et al., 2021).
443 Notably, these were marked with receptors for tissue residency CD103 (*ITGAE*), CD49a
444 (*ITGA1*), chemokine expression (XCL1/2) and lymphocyte exhaustion markers TIM3 (*HAVCR2*),
445 TIGIT, *TNFRSF4*), potentially suggesting conversion of cytotoxic NK cells to an adaptive-like
446 immunomodulatory phenotype that can persist in tissues (Brownlie et al., 2021; Ruckert et
447 al., 2022). Single cell RNAseq from PDAC tissue confirm that trNKs are likely to mediate
448 recruitment of cDC1s via XCL1-XCR1, but communicate additional signals, including IL-16,
449 LIGHT (*TNFSF14*) and MIF-CD74 which have the potential to upregulate MHC-I expression,
450 presentation and co-stimulatory molecules to contribute to cross presentation(Basha et al.,
451 2012; Cruikshank et al., 1987; Zou and Hu, 2005). We also find that trNK may also recruit
452 $CD4^{+}$ Tregs via IL16 but concomitant FAS-signaling would lead to Treg apoptosis and support
453 tumor control (Figure 5E, 6D).
454 Strikingly, using our signature we find that elevated involvement of trNKs in PDAC correlates
455 with CD8 T cell recruitment in a cDC1-dependent manner. Moreover, this supports a model
456 where the inactivation of cytotoxic NK cells in tumors appears to be a conversion to
457 immunomodulatory trNKs and an important mechanistic switch from innate to adaptive
458 immunity. Our therapeutic strategy of short ablative radiation-induced damage (IR) followed

459 by CCR5i/αPD1 (IT) offers a potential regimen to increase disease free survival in PDAC.
460 Finally, trNK-like cells with similar traits are increasingly being observed across a variety of
461 cancers(Brownlie et al., 2023; Kirchhammer et al., 2022; Marquardt et al., 2015). Finally, our
462 signature identifies patients with a significant survival benefit across 14 tumor types,
463 indicating a universal phenomenon attributable to this hypo-cytotoxic immunomodulatory
464 NK subset.

465 ## Author contributions

466 Conceptualization, S.M., EO'N. Methodology, S.L., S.H., C.D. Investigation; S.L., S.H., S.G., C.D. E.AJ.
467 Formal analysis, S.G., S.H., C.D., E.AJ. Data curation, S.G., S.L., S.H., C.D., H.F., S.S. Funding acquisition:
468 M.R.M., J.M, E.O'N. Project administration: E.O'N. Supervision: K.J., E.O'N. Writing – original draft, S.G,
469 C.D, E.O'N. Writing – review & editing, S.G., R.BR., G.V., J.M., K.J., E.O'N. All authors read and
470 approved the manuscript.

471

472 ## Acknowledgements

473 Authors thank the oncology preclinical imaging core (S.Smart, V.Kersemans, PD.Allen, M. Hill
474 and JM Thompson) for providing contracted small animal MRI and radiotherapy services,
475 Biomedical Services (K.Watson) and H. Xu for technical support. Funding: Kidani Memorial
476 Trust, Cancer Research UK, Precision Panc (A25233), CRUK Beatson Institute (A31287,
477 A29996) and CRUK Scotland Centre (CTRQQR-2021\100006). Medical Research Council.

478

479

480 ## References

481 Ajuebor, M. N., Wondimu, Z., Hogaboam, C. M., Le, T., Proudfoot, A. E., and Swain, M. G. (2007).
482 CCR5 deficiency drives enhanced natural killer cell trafficking to and activation within the liver in
483 murine T cell-mediated hepatitis. Am J Pathol *170*, 1975-1988.
484 Aldinucci, D., Borghese, C., and Casagrande, N. (2020). The CCL5/CCR5 Axis in Cancer Progression.
485 Cancers (Basel) *12*.
486 Alshetaiwi, H., Pervolarakis, N., McIntyre, L. L., Ma, D., Nguyen, Q., Rath, J. A., Nee, K., Hernandez,
487 G., Evans, K., Torosian, L.*, et al.* (2020). Defining the emergence of myeloid-derived suppressor cells
488 in breast cancer using single-cell transcriptomics. Sci Immunol *5*.
489 Basha, G., Omilusik, K., Chavez-Steenbock, A., Reinicke, A. T., Lack, N., Choi, K. B., and Jefferies, W. A.
490 (2012). A CD74-dependent MHC class I endolysosomal cross-presentation pathway. Nat Immunol *13*,
491 237-245.
492 Bialecki, E., Macho Fernandez, E., Ivanov, S., Paget, C., Fontaine, J., Rodriguez, F., Lebeau, L., Ehret,
493 C., Frisch, B., Trottein, F., and Faveeuw, C. (2011). Spleen-resident CD4+ and CD4- CD8alpha-
494 dendritic cell subsets differ in their ability to prime invariant natural killer T lymphocytes. PLoS One
495 *6*, e26919.
496 Bockorny, B., Semenisty, V., Macarulla, T., Borazanci, E., Wolpin, B. M., Stemmer, S. M., Golan, T.,
497 Geva, R., Borad, M. J., Pedersen, K. S.*, et al.* (2020). BL-8040, a CXCR4 antagonist, in combination
498 with pembrolizumab and chemotherapy for pancreatic cancer: the COMBAT trial. Nat Med *26*, 878-
499 885.
500 Böttcher, J. P., Bonavita, E., Chakravarty, P., Blees, H., Cabeza-Cabrerizo, M., Sammicheli, S., Rogers,
501 N. C., Sahai, E., Zelenay, S., and Reis e Sousa, C. (2018). NK Cells Stimulate Recruitment of cDC1 into
502 the Tumor Microenvironment Promoting Cancer Immune Control. Cell *172*, 1022-1037.e1014.
503 Brownlie, D., Scharenberg, M., Mold, J. E., Hard, J., Kekalainen, E., Buggert, M., Nguyen, S., Wilson, J.
504 N., Al-Ameri, M., Ljunggren, H. G.*, et al.* (2021). Expansions of adaptive-like NK cells with a tissue-
505 resident phenotype in human lung and blood. Proc Natl Acad Sci U S A *118*.

506 Brownlie, D., von Kries, A., Valenzano, G., Wild, N., Yilmaz, E., Safholm, J., Al-Ameri, M., Alici, E.,
507 Ljunggren, H. G., Schliemann, I*., et al.* (2023). Accumulation of tissue-resident natural killer cells,
508 innate lymphoid cells, and CD8(+) T cells towards the center of human lung tumors.
509 Oncoimmunology *12*, 2233402.
510 Bryceson, Y. T., and Ljunggren, H. G. (2008). Tumor cell recognition by the NK cell activating receptor
511 NKG2D. Eur J Immunol *38*, 2957-2961.
512 Cao, L., Huang, C., Cui Zhou, D., Hu, Y., Lih, T. M., Savage, S. R., Krug, K., Clark, D. J., Schnaubelt, M.,
513 Chen, L*., et al.* (2021). Proteogenomic characterization of pancreatic ductal adenocarcinoma. Cell
514 *184*, 5031-5052 e5026.
515 Caushi, J. X., Zhang, J., Ji, Z., Vaghasia, A., Zhang, B., Hsiue, E. H., Mog, B. J., Hou, W., Justesen, S.,
516 Blosser, R*., et al.* (2021). Transcriptional programs of neoantigen-specific TIL in anti-PD-1-treated
517 lung cancers. Nature *596*, 126-132.
518 Cruikshank, W. W., Berman, J. S., Theodore, A. C., Bernardo, J., and Center, D. M. (1987).
519 Lymphokine activation of T4+ T lymphocytes and monocytes. J Immunol *138*, 3817-3823.
520 de Andrade, L. F., Lu, Y., Luoma, A., Ito, Y., Pan, D., Pyrdol, J. W., Yoon, C. H., Yuan, G. C., and
521 Wucherpfennig, K. W. (2019). Discovery of specialized NK cell populations infiltrating human
522 melanoma metastases. JCI Insight *4*.
523 Di Pilato, M., Kfuri-Rubens, R., Pruessmann, J. N., Ozga, A. J., Messemaker, M., Cadilha, B. L.,
524 Sivakumar, R., Cianciaruso, C., Warner, R. D., Marangoni, F*., et al.* (2021). CXCR6 positions cytotoxic T
525 cells to receive critical survival signals in the tumor microenvironment. Cell *184*, 4512-4530 e4522.
526 Doi, T., Muro, K., Ishii, H., Kato, T., Tsushima, T., Takenoyama, M., Oizumi, S., Gemmoto, K., Suna, H.,
527 Enokitani, K*., et al.* (2019). A Phase I Study of the Anti-CC Chemokine Receptor 4 Antibody,
528 Mogamulizumab, in Combination with Nivolumab in Patients with Advanced or Metastatic Solid
529 Tumors. Clin Cancer Res *25*, 6614-6622.
530 Groh, V., Wu, J., Yee, C., and Spies, T. (2002). Tumour-derived soluble MIC ligands impair expression
531 of NKG2D and T-cell activation. Nature *419*, 734-738.
532 Hashemi, E., and Malarkannan, S. (2020). Tissue-Resident NK Cells: Development, Maturation, and
533 Clinical Relevance. Cancers (Basel) *12*.
534 Hemmatazad, H., and Berger, M. D. (2021). CCR5 is a potential therapeutic target for cancer. Expert
535 Opin Ther Targets *25*, 311-327.
536 Huang, H., Zepp, M., Georges, R. B., Jarahian, M., Kazemi, M., Eyol, E., and Berger, M. R. (2020). The
537 CCR5 antagonist maraviroc causes remission of pancreatic cancer liver metastasis in nude rats based
538 on cell cycle inhibition and apoptosis induction. Cancer Lett *474*, 82-93.
539 Jin, S., Guerrero-Juarez, C. F., Zhang, L., Chang, I., Ramos, R., Kuan, C. H., Myung, P., Plikus, M. V., and
540 Nie, Q. (2021). Inference and analysis of cell-cell communication using CellChat. Nat Commun *12*,
541 1088.
542 Kaiser, B. K., Yim, D., Chow, I. T., Gonzalez, S., Dai, Z., Mann, H. H., Strong, R. K., Groh, V., and Spies,
543 T. (2007). Disulphide-isomerase-enabled shedding of tumour-associated NKG2D ligands. Nature *447*,
544 482-486.
545 Kaser, A., Dunzendorfer, S., Offner, F. A., Ryan, T., Schwabegger, A., Cruikshank, W. W.,
546 Wiedermann, C. J., and Tilg, H. (1999). A role for IL-16 in the cross-talk between dendritic cells and T
547 cells. J Immunol *163*, 3232-3238.
548 Kirchhammer, N., Trefny, M. P., Natoli, M., Brucher, D., Smith, S. N., Werner, F., Koch, V., Schreiner,
549 D., Bartoszek, E., Buchi, M*., et al.* (2022). NK cells with tissue-resident traits shape response to
550 immunotherapy by inducing adaptive antitumor immunity. Sci Transl Med *14*, eabm9043.
551 Lander, V. E., Belle, J. I., Kingston, N. L., Herndon, J. M., Hogg, G. D., Liu, X., Kang, L. I., Knolhoff, B. L.,
552 Bogner, S. J., Baer, J. M*., et al.* (2022). Stromal Reprogramming by FAK Inhibition Overcomes
553 Radiation Resistance to Allow for Immune Priming and Response to Checkpoint Blockade. Cancer
554 Discov *12*, 2774-2799.
555 Lopez-Botet, M., De Maria, A., Muntasell, A., Della Chiesa, M., and Vilches, C. (2023). Adaptive NK
556 cell response to human cytomegalovirus: Facts and open issues. Semin Immunol *65*, 101706.

557 Marcon, F., Zuo, J., Pearce, H., Nicol, S., Margielewska-Davies, S., Farhat, M., Mahon, B., Middleton,
558 G., Brown, R., Roberts, K. J., and Moss, P. (2020). NK cells in pancreatic cancer demonstrate impaired
559 cytotoxicity and a regulatory IL-10 phenotype. Oncoimmunology *9*, 1845424.
560 Marquardt, N., Beziat, V., Nystrom, S., Hengst, J., Ivarsson, M. A., Kekalainen, E., Johansson, H.,
561 Mjosberg, J., Westgren, M., Lankisch, T. O.*, et al.* (2015). Cutting edge: identification and
562 characterization of human intrahepatic CD49a+ NK cells. J Immunol *194*, 2467-2471.
563 Matzke-Ogi, A., Jannasch, K., Shatirishvili, M., Fuchs, B., Chiblak, S., Morton, J., Tawk, B., Lindner, T.,
564 Sansom, O., Alves, F.*, et al.* (2016). Inhibition of Tumor Growth and Metastasis in Pancreatic Cancer
565 Models by Interference With CD44v6 Signaling. Gastroenterology *150*, 513-525 e510.
566 Mijnheer, G., Lutter, L., Mokry, M., van der Wal, M., Scholman, R., Fleskens, V., Pandit, A., Tao, W.,
567 Wekking, M., Vervoort, S.*, et al.* (2021). Conserved human effector Treg cell transcriptomic and
568 epigenetic signature in arthritic joint inflammation. Nat Commun *12*, 2710.
569 Mills, B. N., Qiu, H., Drage, M. G., Chen, C., Mathew, J. S., Garrett-Larsen, J., Ye, J., Uccello, T. P.,
570 Murphy, J. D., Belt, B. A.*, et al.* (2022). Modulation of the Human Pancreatic Ductal Adenocarcinoma
571 Immune Microenvironment by Stereotactic Body Radiotherapy. Clin Cancer Res *28*, 150-162.
572 Mohindra, N. A., Kircher, S. M., Nimeiri, H. S., Benson, A. B., Rademaker, A., Alonso, E., Blatner, N.,
573 Khazaie, K., and Mulcahy, M. F. (2015). Results of the phase Ib study of ipilimumab and gemcitabine
574 for advanced pancreas cancer. Journal of Clinical Oncology *33*, e15281-e15281.
575 Monti, P., Marchesi, F., Reni, M., Mercalli, A., Sordi, V., Zerbi, A., Balzano, G., Di Carlo, V., Allavena,
576 P., and Piemonti, L. (2004). A comprehensive in vitro characterization of pancreatic ductal carcinoma
577 cell line biological behavior and its correlation with the structural and genetic profile. Virchows Arch
578 *445*, 236-247.
579 Nersesian, S., Schwartz, S. L., Grantham, S. R., MacLean, L. K., Lee, S. N., Pugh-Toole, M., and
580 Boudreau, J. E. (2021). NK cell infiltration is associated with improved overall survival in solid
581 cancers: A systematic review and meta-analysis. Transl Oncol *14*, 100930.
582 Parikh, A. R., Szabolcs, A., Allen, J. N., Clark, J. W., Wo, J. Y., Raabe, M., Thel, H., Hoyos, D., Mehta, A.,
583 Arshad, S.*, et al.* (2021). Radiation therapy enhances immunotherapy response in microsatellite
584 stable colorectal and pancreatic adenocarcinoma in a phase II trial. Nat Cancer *2*, 1124-1135.
585 Peng, Y. P., Zhu, Y., Zhang, J. J., Xu, Z. K., Qian, Z. Y., Dai, C. C., Jiang, K. R., Wu, J. L., Gao, W. T., Li, Q.*,*
586 *et al.* (2013). Comprehensive analysis of the percentage of surface receptors and cytotoxic granules
587 positive natural killer cells in patients with pancreatic cancer, gastric cancer, and colorectal cancer. J
588 Transl Med *11*, 262.
589 Piper, M., Hoen, M., Darragh, L. B., Knitz, M. W., Nguyen, D., Gadwa, J., Durini, G., Karakoc, I., Grier,
590 A., Neupert, B.*, et al.* (2023). Simultaneous targeting of PD-1 and IL-2Rbetagamma with radiation
591 therapy inhibits pancreatic cancer growth and metastasis. Cancer Cell *41*, 950-969 e956.
592 Poli, A., Michel, T., Theresine, M., Andres, E., Hentges, F., and Zimmer, J. (2009). CD56bright natural
593 killer (NK) cells: an important NK cell subset. Immunology *126*, 458-465.
594 Quatrini, L., Molfetta, R., Zitti, B., Peruzzi, G., Fionda, C., Capuano, C., Galandrini, R., Cippitelli, M.,
595 Santoni, A., and Paolini, R. (2015). Ubiquitin-dependent endocytosis of NKG2D-DAP10 receptor
596 complexes activates signaling and functions in human NK cells. Sci Signal *8*, ra108.
597 Rand, T. H., Cruikshank, W. W., Center, D. M., and Weller, P. F. (1991). CD4-mediated stimulation of
598 human eosinophils: lymphocyte chemoattractant factor and other CD4-binding ligands elicit
599 eosinophil migration. J Exp Med *173*, 1521-1528.
600 Royal, R. E., Levy, C., Turner, K., Mathur, A., Hughes, M., Kammula, U. S., Sherry, R. M., Topalian, S.
601 L., Yang, J. C., Lowy, I., and Rosenberg, S. A. (2010). Phase 2 trial of single agent Ipilimumab (anti-
602 CTLA-4) for locally advanced or metastatic pancreatic adenocarcinoma. J Immunother *33*, 828-833.
603 Ruckert, T., Lareau, C. A., Mashreghi, M. F., Ludwig, L. S., and Romagnani, C. (2022). Clonal expansion
604 and epigenetic inheritance of long-lasting NK cell memory. Nat Immunol *23*, 1551-1563.
605 Simhadri, V. R., Reiners, K. S., Hansen, H. P., Topolar, D., Simhadri, V. L., Nohroudi, K., Kufer, T. A.,
606 Engert, A., and Pogge von Strandmann, E. (2008). Dendritic cells release HLA-B-associated transcript-
607 3 positive exosomes to regulate natural killer function. PLoS One *3*, e3377.

608 Singh, S. K., Mishra, M. K., Eltoum, I. A., Bae, S., Lillard, J. W., Jr., and Singh, R. (2018). CCR5/CCL5 axis
609 interaction promotes migratory and invasiveness of pancreatic cancer cells. Sci Rep *8*, 1323.
610 Siolas, D., Morrissey, C., and Oberstein, P. E. (2020). The Achilles' Heel of Pancreatic Cancer:
611 Targeting pancreatic cancer's unique immunologic characteristics and metabolic dependencies in
612 clinical trials. J Pancreatol *3*, 121-131.
613 Smith, S. L., Kennedy, P. R., Stacey, K. B., Worboys, J. D., Yarwood, A., Seo, S., Solloa, E. H., Mistretta,
614 B., Chatterjee, S. S., Gunaratne, P.*, et al.* (2020). Diversity of peripheral blood human NK cells
615 identified by single-cell RNA sequencing. Blood Adv *4*, 1388-1406.
616 Sodergren, M. H., Mangal, N., Wasan, H., Sadanandam, A., Balachandran, V. P., Jiao, L. R., and Habib,
617 N. (2020). Immunological combination treatment holds the key to improving survival in pancreatic
618 cancer. J Cancer Res Clin Oncol *146*, 2897-2911.
619 Steele, C. W., Karim, S. A., Foth, M., Rishi, L., Leach, J. D., Porter, R. J., Nixon, C., Jeffry Evans, T. R.,
620 Carter, C. R., Nibbs, R. J.*, et al.* (2015). CXCR2 inhibition suppresses acute and chronic pancreatic
621 inflammation. J Pathol *237*, 85-97.
622 Steele, N. G., Carpenter, E. S., Kemp, S. B., Sirihorachai, V. R., The, S., Delrosario, L., Lazarus, J., Amir,
623 E. D., Gunchick, V., Espinoza, C.*, et al.* (2020). Multimodal Mapping of the Tumor and Peripheral
624 Blood Immune Landscape in Human Pancreatic Cancer. Nat Cancer *1*, 1097-1112.
625 Tan, M. C., Goedegebuure, P. S., Belt, B. A., Flaherty, B., Sankpal, N., Gillanders, W. E., Eberlein, T. J.,
626 Hsieh, C. S., and Linehan, D. C. (2009). Disruption of CCR5-dependent homing of regulatory T cells
627 inhibits tumor growth in a murine model of pancreatic cancer. J Immunol *182*, 1746-1755.
628 Uhlen, M., Zhang, C., Lee, S., Sjostedt, E., Fagerberg, L., Bidkhori, G., Benfeitas, R., Arif, M., Liu, Z.,
629 Edfors, F.*, et al.* (2017). A pathology atlas of the human cancer transcriptome. Science *357*.
630 Vremec, D., Pooley, J., Hochrein, H., Wu, L., and Shortman, K. (2000). CD4 and CD8 expression by
631 dendritic cell subtypes in mouse thymus and spleen. J Immunol *164*, 2978-2986.
632 Wang, J., Saung, M. T., Li, K., Fu, J., Fujiwara, K., Niu, N., Muth, S., Wang, J., Xu, Y., Rozich, N.*, et al.*
633 (2022). CCR2/CCR5 inhibitor permits the radiation-induced effector T cell infiltration in pancreatic
634 adenocarcinoma. J Exp Med *219*.
635 Wang, L., He, T., Liu, J., Tai, J., Wang, B., Chen, Z., and Quan, Z. (2021). Pan-cancer analysis reveals
636 tumor-associated macrophage communication in the tumor microenvironment. Exp Hematol Oncol
637 *10*, 31.
638 Weiss, G. J., Blaydorn, L., Beck, J., Bornemann-Kolatzki, K., Urnovitz, H., Schutz, E., and Khemka, V.
639 (2018). Phase Ib/II study of gemcitabine, nab-paclitaxel, and pembrolizumab in metastatic pancreatic
640 adenocarcinoma. Invest New Drugs *36*, 96-102.
641 Weiss, G. J., Waypa, J., Blaydorn, L., Coats, J., McGahey, K., Sangal, A., Niu, J., Lynch, C. A., Farley, J.
642 H., and Khemka, V. (2017). A phase Ib study of pembrolizumab plus chemotherapy in patients with
643 advanced cancer (PembroPlus). Br J Cancer *117*, 33-40.
644 Willenbrock, F., Cox, C. M., Parkes, E. E., Wilhelm-Benartzi, C. S., Abraham, A. G., Owens, R.,
645 Sabbagh, A., Jones, C. M., Hughes, D. L. I., Maughan, T.*, et al.* (2021). Circulating biomarkers and
646 outcomes from a randomised phase 2 trial of gemcitabine versus capecitabine-based
647 chemoradiotherapy for pancreatic cancer. Br J Cancer *124*, 581-586.
648 Wu, S. Y., Fu, T., Jiang, Y. Z., and Shao, Z. M. (2020). Natural killer cells in cancer biology and therapy.
649 Mol Cancer *19*, 120.
650 Zou, G. M., and Hu, W. Y. (2005). LIGHT regulates CD86 expression on dendritic cells through NF-
651 kappaB, but not JNK/AP-1 signal transduction pathway. J Cell Physiol *205*, 437-443.

652

653

654 **Figure 1.** (A) Overall and disease-free Kaplan-Meier survival plots of PDAC patients segregated
655 into high or low CCL5 gene expression levels within pancreatic tumors. Data are derived from
656 CTPAC3 and TCGA cohorts and optimal cut-off values were calculated using the max-stat
657 method for each respective cohort. (B) Schematic overview of CCL5-responsive immune cells
658 and corresponding CCL5 receptor repertoire expression. (C) Correlation between overall and
659 single cell gene signatures of CCL5-responsive immune cells with overall PDAC prognosis.
660 Colour depicts positive (green), negative (red) or neutral (black) prognostic outcomes
661 (*p<0.05, ** p<0.01, *** p<0.005) . Data are derived from the Pathology Dataset of the
662 Human Protein Atlas19 and based on human tissue micro arrays and correlated log-rank p
663 value for Kaplan Meier analysis.
664 **Figure 2.** (A) Three different lineages of KPC pancreatic tumor cells (derived from
665 KrasG12Dp53R172HPdx1-Cre mice) were obtained and stained for DAPI (blue; nucleus), E-
666 cadherin (green; epithelial) and Vimentin (red; mesenchymal). Growth curve of orthotopically
667 injected KPC-F cells (500 cells) into the pancreas of wildtype C57BL/6 over time in weeks.
668 Tumor volume was measured using MRI. Representative MRI images over time are displayed,
669 white arrow denotes tumor mass. (B) Timeline of maraviroc (anti-CCR5) treatment regimen.
670 A total of 12 days post-orthotopic injection, tumor-bearing mice were treated daily with
671 maraviroc (10 mg/kg via intraperitoneal injection) for 6 days and followed for up to 30 days
672 after starting treatment. Frequencies of pancreatic tumor-infiltrating immune cells harvested
673 at day 30 with or without maraviroc using Aurora Cytek spectral flow is shown. Data are
674 represented as mean percentage positive cells (of CD45) ± SD. Significance was tested using
675 the Welch and Brown-Forsythe ANOVA for parametric data or Kruskal-Wallis test for non-
676 parametric data. Mock (n=6), IR (n=3), aPD1 (n=8), aPD1+IR (n=8), CCR5i (n=3), CCR5i+IR
677 (n=8), aPD1+CCR5i (n=5), aPD1+CCR5i+IR (n=8).
678 **Figure 3.** (A) Timeline of triple treatment regimen (maraviroc, αPD1 and radiotherapy)
679 following orthotopic injection of KPC_F cells. A total of 12 days post orthotopic injection of
680 500 KPC-F cells in the pancreas of wildtype C57BL/6 mice, mice were treated as follows:
681 seven consecutive days of 10 mg/kg intraperitoneal injection of maraviroc and four
682 alternating days of 10 mg/kg intraperitoneal injection of αPD1. Mice were followed for up to
683 30 days following the start of the treatment regimen. Tumor volumes were measured by MRI
684 and growth curves of individual treatment groups are plotted with or without radiotherapy as
685 measured by MRI. Average growth curves ± SD are depicted in bold, individual mice are

686 shaded (without IR; dashed, with IR; solid). Insert: expanded view of triple combination to
687 show 'responders' display a significant benefit over RT alone. (B) Quantification of pancreatic
688 tumors derived from (A) stained by IHC for p53. (C) Quantification of necrotic areas in
689 pancreatic tumors derived from (A) based on H&E staining. (D) Quantification of infiltrating
690 CD8+ in pancreatic tumors derived from (A) by flow cytometry. (E) Profiling of infiltrating
691 immune cells in pancreatic tumors derived from (A) by Aurora Cytek as in figure 2B. Single,
692 live cells were included for analysis and are represented as frequencies of CD45+ cells or total
693 CD3+ for Foxp3+ Tregs. Significance was tested using the Welch and Brown-Forsythe ANOVA
694 for parametric data # $p<0.05$, ##$p<0.01$ or Kruskal-Wallis test for non-parametric data #w
695 $p<0.01$; pairwise comparisons (student t test) *$p<0.05$, **$p<0.01$, ***$p<0.005$, ****$p<0.001$.
696 **Figure 4.** (A) Spatial plots of individual cells identified using HALO software of scanned
697 multiplex immunofluorescence murine pancreatic tumor slices. Positive staining is identified
698 as the marker of interest and DAPI+ signal. Responders and non-responders to treatment are
699 based on loss of E-cadherin staining. (B) Percentages of total DAPI+ immune cells (left) and E-
700 cadherin+ tumor cells (right) derived from Figure 4A following treatment. Significance was
701 tested using two-way ANOVA with Tukey multiple comparison (blue significance lines), or
702 one-way ANOVA with Tukey multiple comparison (yellow significance lines) using a $p<0.05$.
703 Correlations between %positive immune cells plotted against %positive E-cadherin+ cells, as
704 derived from (A). Symbols and colours represent different treatment groups. (C) Correlation
705 of total CD4 T (CD3+CD8-), CD8 T (CD3+CD8+) and NK cells (CD3-NK1.1+) plotted against
706 %positive E-cadherin+ cells as derived from (A). (D) Correlation of %positive segregated NK
707 cells plotted against %positive E-cadherin+ cells as derived from (A). NK cells were segregated
708 based on expression of NKG2D; NKActive; NK1.1+NKG2D+; NKNKG2D-ve; NK1.1+NKG2D-. (E)
709 Intratumoral immune cells of stratified pancreatic tumors based on low or high E-cadherin
710 percentage (cut-off: 20%). Significance was tested for $p<0.05$ with a two-tailed student's T-
711 test. * censored non-responder.
712 **Figure 5.** (A) UMAP of the CD8+ T and NK sub-clusters from Steele et al (arrows illustrate the
713 developmental path of NK cells). (B) Dot plot showing the expression of exhaustion-related
714 genes across CD8+ T and NK sub-clusters. (C) Dot plot showing highly expressed genes for
715 each sub-cluster. (D) UMAP of the three NK subclusters (left), and violin plots comparing the
716 expression of NK subtype-associated genes between the sub-clusters (right). (E) Dot plot

717 showing the different gene expression programs across the three NK sub-clusters. (F)
718 Heatmap showing the top 15 upregulated markers for each NK sub-cluster.
719 **Figure 6.** (A) UMAP of the dendritic cell sub-clusters from the Steele dataset. (B) Violin plot
720 showing the expression of XCL1, XCL2, and XCR1 across all cell types. (C) Circle plots showing
721 interactions across all cell types (top left), signals coming from the tissue-resident NK cells
722 (top right), the XCL1-XCR1 interaction (bottom left), and the XCL2-XCR1 interaction (bottom
723 right). The width of edges represents the communication strength. (D) Heatmap showing the
724 summary of secreted signalling communications of outgoing (left) and incoming (right)
725 signals. The colour bar represents the communication strength, and the size of the bars
726 represents the sum of signalling strength for each pathway or cell type. (E) Schematic
727 overview of the trNK to cDC1 and cDC1 to CD8 T cell communication axis (top). Circle plots of
728 all outgoing signals from cDC1 (bottom left) and the CXCL16-CXCR6 signalling (bottom right).
729 (F) Correlation of HALO data on total NKNKG2D-ve/trNK cells (CD3-NK1.1+NKG2D-) with CD8
730 T (CD3+CD8+) from stained sections of treated KPC_F orthotopic tumors, R2 and p values
731 indicate positive correlation across all tumors (gray, n=15) or limited to mock, CCR5i IR and
732 CCR5i aPD1 IR combination (red, n =9). (G) Correlation of trNK signature with CD8A (left) or
733 CD8B (right) in bulk RNAseq from TCGA_PAAD and binned into quartiles based on extent of
734 cDC1 involvement as assume by cDC1 signature.
735 **Figure 7.** (A) Overall survival analysis correlating CD56 low/high expression with and without
736 radiation therapy in the TCGA dataset. (B) Overall survival analysis correlating the
737 deconvoluted NK C1 signature split into low and high. (C) Overall survival analysis correlating
738 NK C1 low/high enrichment with and without radiation therapy in the TCGA dataset. (D)
739 Boxplot correlating low and high CCL5 expression with NK C1 enrichment score in the TCGA
740 (left) and CPTAC (right) datasets. (E) Overall (left) and disease-free survival (right) analysis of
741 CCL5high patients segregated based on high/low enrichment of trNK (NK_C1) gene signature.
742 (F) Overall survival of CCL5high segregated on CD56 (NCAM1) expression.
743 **Figure 8.** Correlation of tissue-resident NK cells gene signature in human cancer
744 The trNK cell gene signature is a positive prognostic factor across various malignancies using
745 the TCGA_PAAD dataset.
746

Figure 1

A

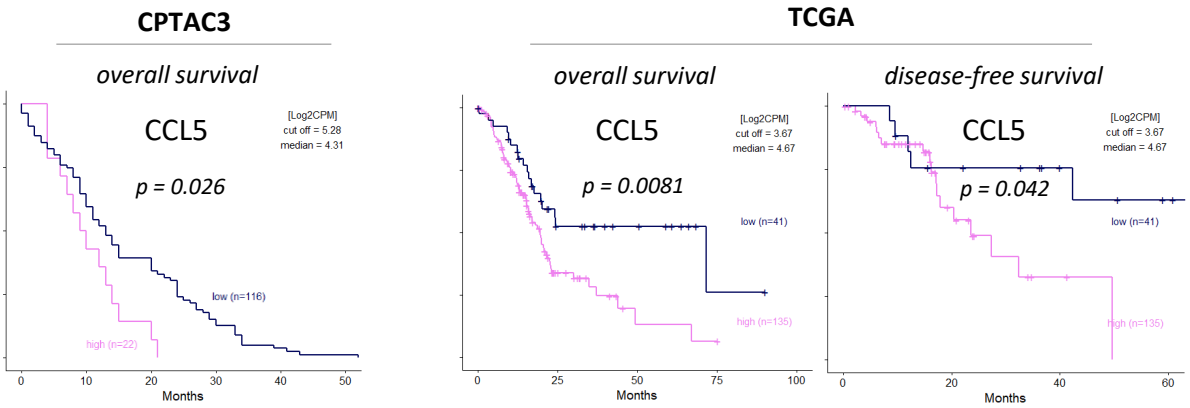

B

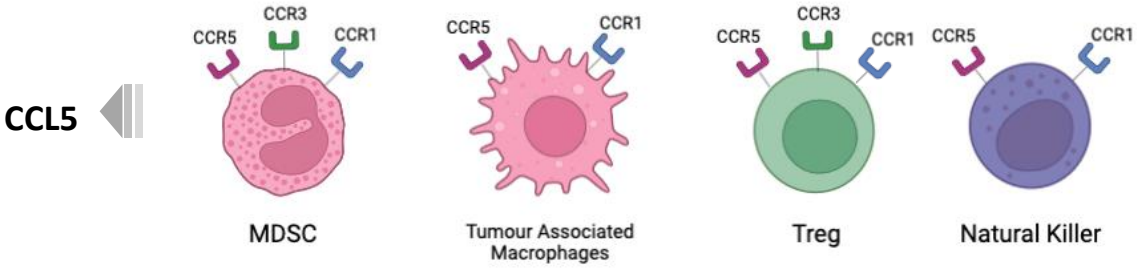

C

Human SCS signature genes

G-MDSC	p-value	M-MDSC	p-value	TAMs	p-value	Treg	p-value	NK	p-value
G-MDSC SCS sig	**ns**	M-MDSC SCS sig	**ns**	TAM SCS sig	**ns**	Treg SCS sig	**ns**	NK SCS sig	**ns**
S100P	***0.0002***	***PLBD1***	***0.00017***	MMP12	***	IKZF2	*	GZMB	*
IFITM2	***	VCAN	***	CD80	*	BLIMP1	*	PRF1	*
RNF24	**	SLC2A3	**	IL1β	*	CTLA4	ns	CD16	*
MME	**	S100A8	*	CCL13	*	TIGIT	ns	KIR	ns
CXCR2	ns	CSF3R	ns	APOE	ns	GITR	ns	NKG2A	ns
LIMK2	ns	FCN1	ns	IL12RB1	ns	BATF	ns	SELL	ns
GCA	ns	LYZ	ns	FLI1	*	IL2RA	ns	NKG2D	*
XPO6	ns	SELL	ns	SEPP1	*	FOXP3	**	CCR7	*
ARG2	***	ARG2	***	GPX3	**	BACH2	***	***CD56***	***0.0000091***

Figure 2

A

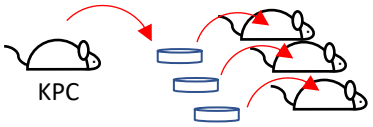
KPC

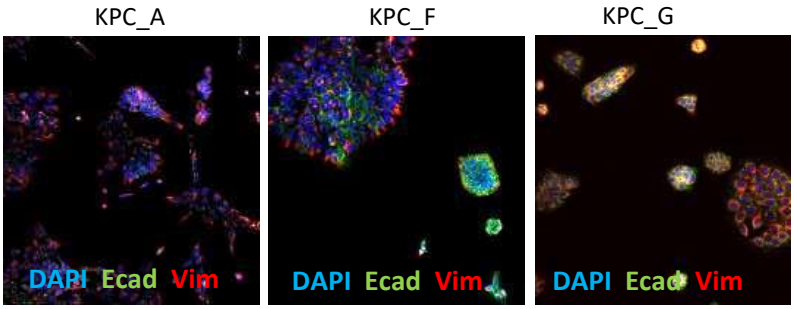
KPC_A
KPC_F
KPC_G
DAPI Ecad Vim
DAPI Ecad Vim
DAPI Ecad Vim

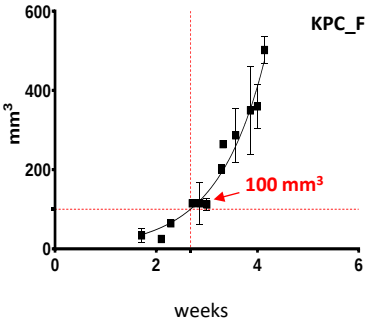
KPC_F
600
400
200
0
mm³
100 mm³
0
2
4
6
weeks

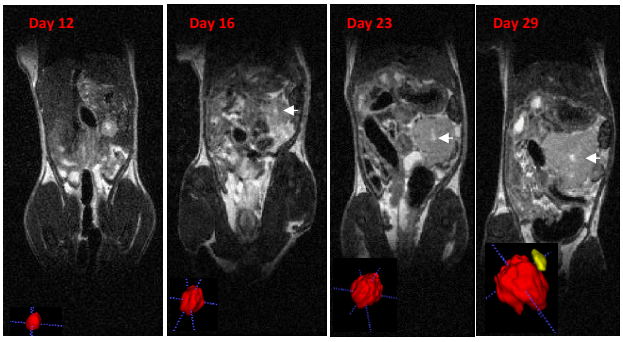
Day 12
Day 16
Day 23
Day 29

B

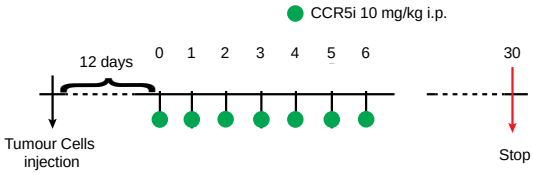
CCR5i 10 mg/kg i.p.
12 days
0 1 2 3 4 5 6
30
Tumour Cells injection
Stop

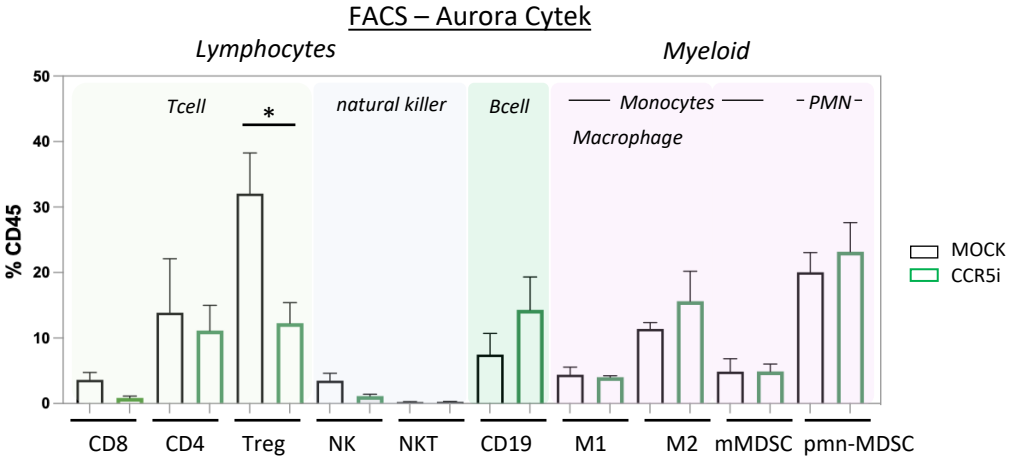
FACS – Aurora Cytek
Lymphocytes
Myeloid
Tcell
*
natural killer
Bcell
Monocytes
PMN
Macrophage
% CD45
50
40
30
20
10
0
MOCK
CCR5i
CD8
CD4
Treg
NK
NKT
CD19
M1
M2
mMDSC
pmn-MDSC

Figure 3

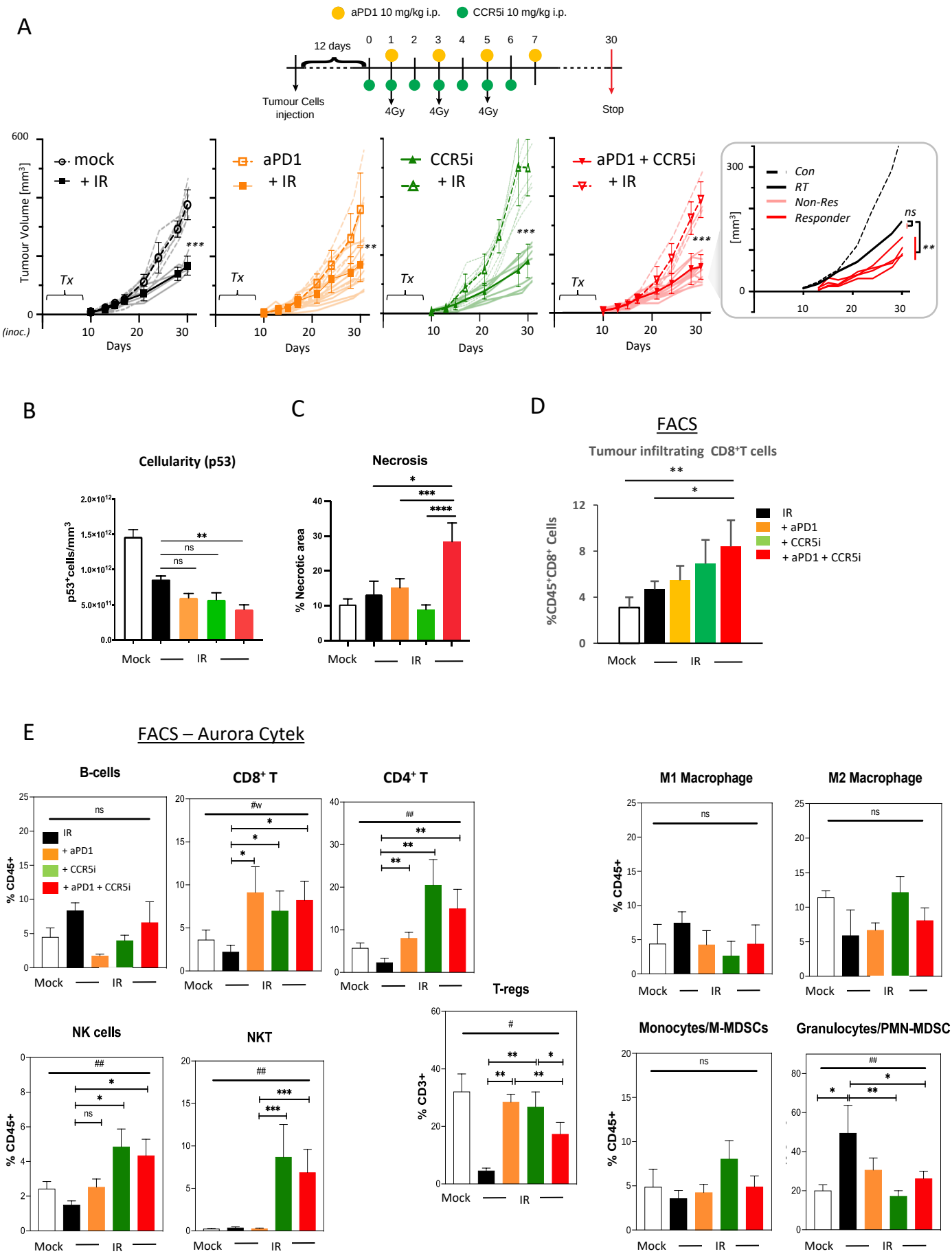
A
aPD1 10 mg/kg i.p.
CCR5i 10 mg/kg i.p.
12 days
0 1 2 3 4 5 6 7 30
Tumour Cells injection
4Gy 4Gy 4Gy
Stop
Tumour Volume [mm³]
mock
+ IR
aPD1
+ IR
CCR5i
+ IR
aPD1 + CCR5i
+ IR
Tx
(inoc.)
Days
Con
RT
Non-Res
Responder
ns
B
Cellularity (p53)
p53⁺cells/mm³
Mock
IR
C
Necrosis
% Necrotic area
D
FACS
Tumour infiltrating CD8⁺T cells
%CD45⁺CD8⁺ Cells
IR
+ aPD1
+ CCR5i
+ aPD1 + CCR5i
E
FACS – Aurora Cytek
B-cells
CD8⁺ T
CD4⁺ T
M1 Macrophage
M2 Macrophage
% CD45+
NK cells
NKT
T-regs
% CD3+
Monocytes/M-MDSCs
Granulocytes/PMN-MDSC

Figure 4

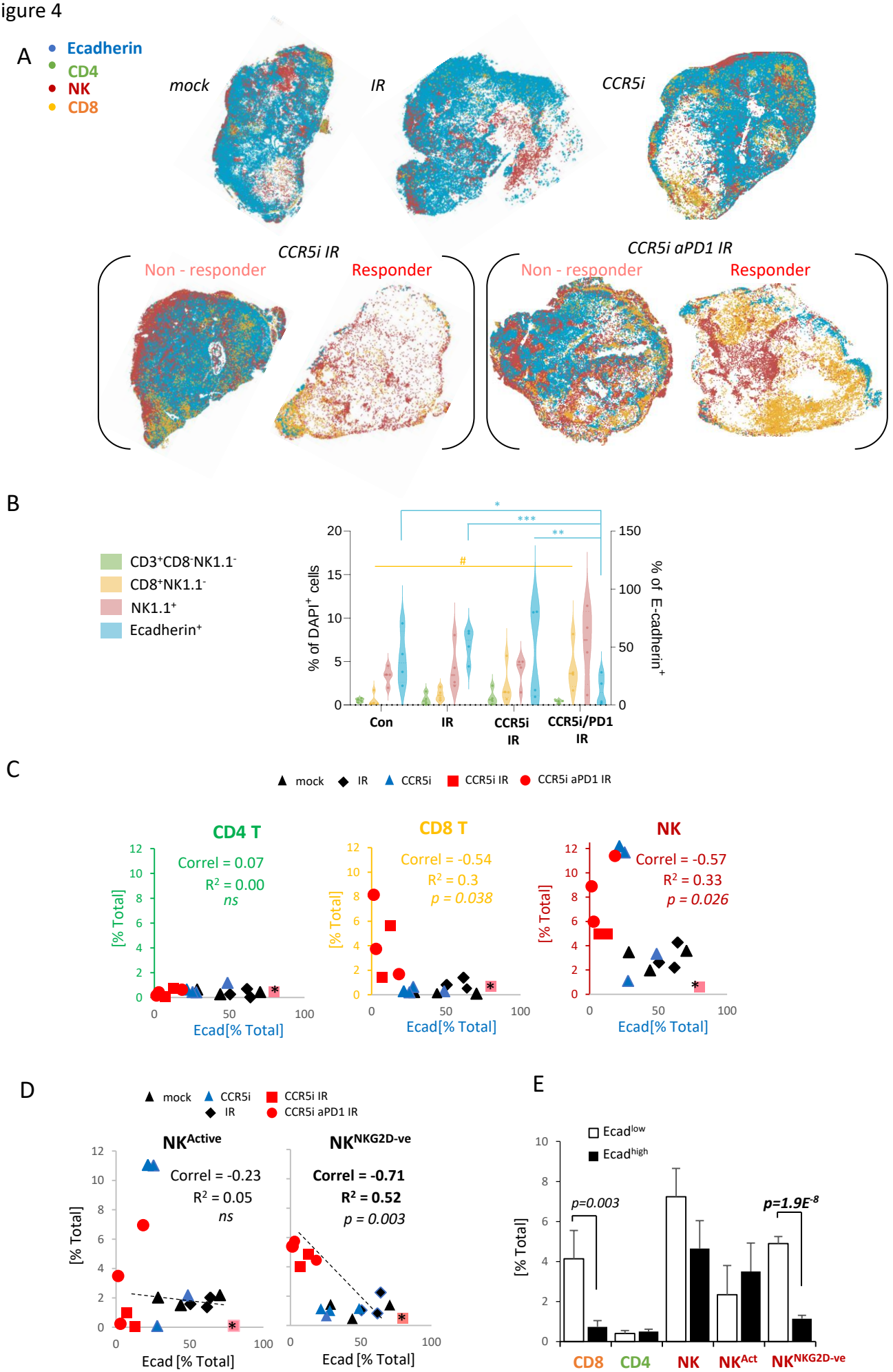
A
Ecadherin
CD4
NK
CD8
mock
IR
CCR5i
CCR5i IR
Non - responder
Responder
CCR5i aPD1 IR
Non - responder
Responder
B
CD3+CD8-NK1.1-
CD8+NK1.1-
NK1.1+
Ecadherin+
% of DAPI+ cells
% of E-cadherin+
Con
IR
CCR5i IR
CCR5i/PD1 IR
C
mock
IR
CCR5i
CCR5i IR
CCR5i aPD1 IR
CD4 T
Correl = 0.07
R2 = 0.00
ns
CD8 T
Correl = -0.54
R2 = 0.3
p = 0.038
NK
Correl = -0.57
R2 = 0.33
p = 0.026
[% Total]
Ecad[% Total]
D
mock
CCR5i
IR
CCR5i IR
CCR5i aPD1 IR
NKActive
Correl = -0.23
R2 = 0.05
ns
NKNKG2D-ve
Correl = -0.71
R2 = 0.52
p = 0.003
[% Total]
Ecad [% Total]
E
Ecadlow
Ecadhigh
p=0.003
p=1.9E-8
[% Total]
CD8
CD4
NK
NKAct
NKNKG2D-ve

Figure 5

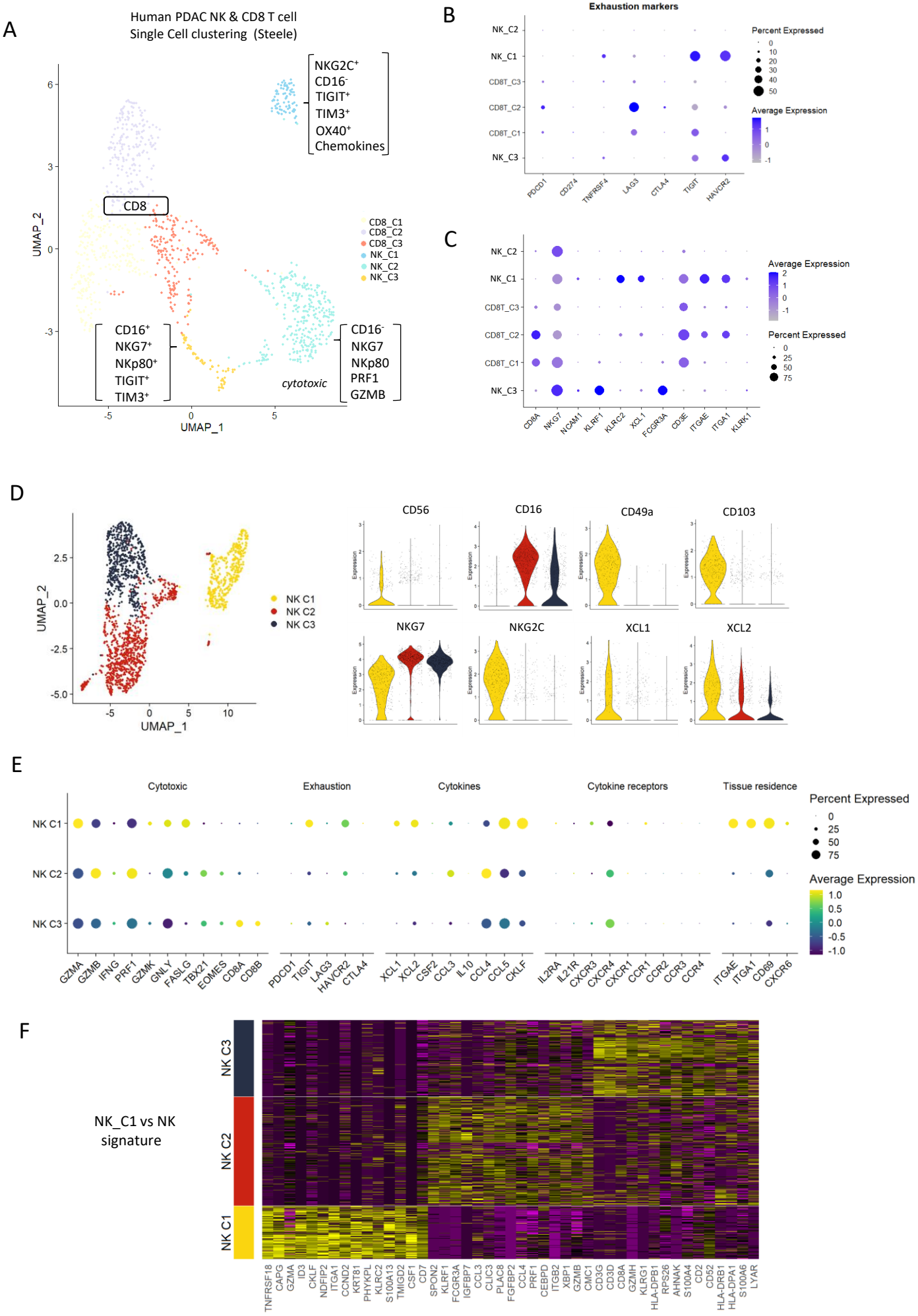
A
Human PDAC NK & CD8 T cell
Single Cell clustering (Steele)
NKG2C+
CD16-
TIGIT+
TIM3+
OX40+
Chemokines
CD8
CD8_C1
CD8_C2
CD8_C3
NK_C1
NK_C2
NK_C3
CD16+
NKG7+
NKp80+
TIGIT+
TIM3+
cytotoxic
CD16-
NKG7
NKp80
PRF1
GZMB
UMAP_2
UMAP_1
B
Exhaustion markers
NK_C2
NK_C1
CD8T_C3
CD8T_C2
CD8T_C1
NK_C3
PDCD1
CD274
TNFRSF4
LAG3
CTLA4
TIGIT
HAVCR2
Percent Expressed
Average Expression
C
NK_C2
NK_C1
CD8T_C3
CD8T_C2
CD8T_C1
NK_C3
CD8A
NKG7
NCAM1
KLRF1
KLRC2
XCL1
FCGR3A
CD3E
ITGAE
ITGA1
KLRK1
Average Expression
Percent Expressed
D
UMAP_2
UMAP_1
NK C1
NK C2
NK C3
CD56
CD16
CD49a
CD103
NKG7
NKG2C
XCL1
XCL2
Expression
E
Cytotoxic
Exhaustion
Cytokines
Cytokine receptors
Tissue residence
NK C1
NK C2
NK C3
GZMA
GZMB
IFNG
PRF1
GZMK
GNLY
FASLG
TBX21
EOMES
CD8A
CD8B
PDCD1
TIGIT
LAG3
HAVCR2
CTLA4
XCL1
XCL2
CSF2
CCL3
IL10
CCL4
CCL5
CKLF
IL2RA
IL21R
CXCR3
CXCR4
CXCR1
CCR1
CCR2
CCR3
CCR4
ITGAE
ITGA1
CD69
CXCR6
Percent Expressed
Average Expression
F
NK_C1 vs NK signature
NK C3
NK C2
NK C1
TNFRSF18
CAPG
GZMA
ID3
CKLF
NDFIP2
ITGA1
CCND2
KRT81
PHYKPL
KLRC2
S100A13
TMIGD2
CSF1
CD7
SPON2
KLRF1
FCGR3A
IGFBP7
CCL3
CLIC3
PLAC8
FGFBP2
CCL4
PRF1
CEBPD
ITGB2
XBP1
GZMB
CMC1
CD3G
CD3D
CD8A
GZMH
KLRG1
HLA-DPB1
RPS26
AHNAK
S100A4
CD2
CD52
HLA-DRB1
HLA-DPA1
S100A6
LYAR

Figure 6

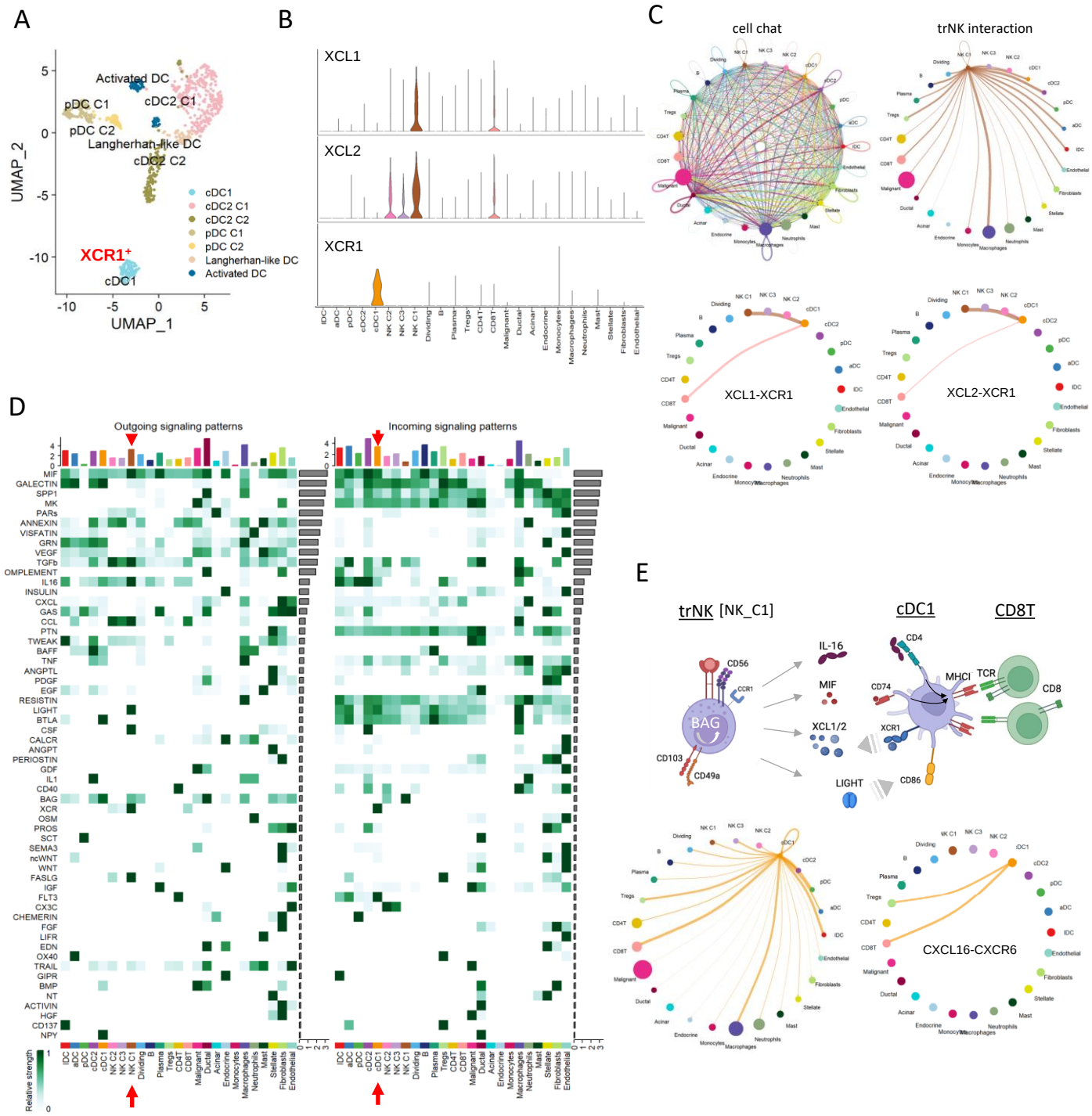
A
Activated DC
pDC C1
cDC2 C1
pDC C2
Langerhan-like DC
cDC2 C2
XCR1+
cDC1
UMAP_2
UMAP_1
cDC1
cDC2 C1
cDC2 C2
pDC C1
pDC C2
Langerhan-like DC
Activated DC
B
XCL1
XCL2
XCR1
C
cell chat
trNK interaction
XCL1-XCR1
XCL2-XCR1
D
Outgoing signaling patterns
Incoming signaling patterns
Relative strength
E
trNK [NK_C1]
cDC1
CD8T
CD56
CCR1
BAG
CD103
CD49a
IL-16
MIF
XCL1/2
LIGHT
CD4
CD74
MHCI
TCR
CD8
XCR1
CD86
CXCL16-CXCR6

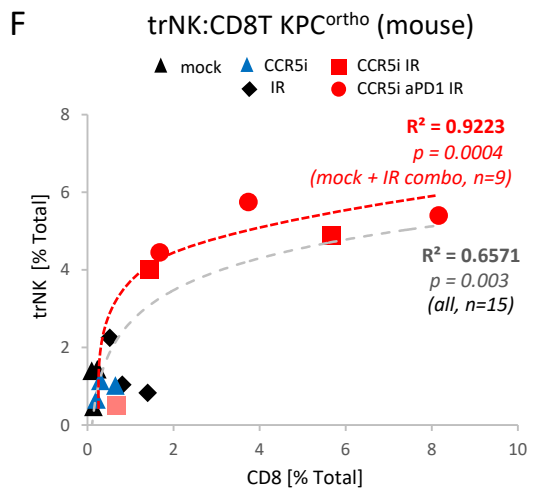
F
trNK:CD8T KPCortho (mouse)
mock
CCR5i
CCR5i IR
IR
CCR5i aPD1 IR
R² = 0.9223
p = 0.0004
(mock + IR combo, n=9)
R² = 0.6571
p = 0.003
(all, n=15)
trNK [% Total]
CD8 [% Total]

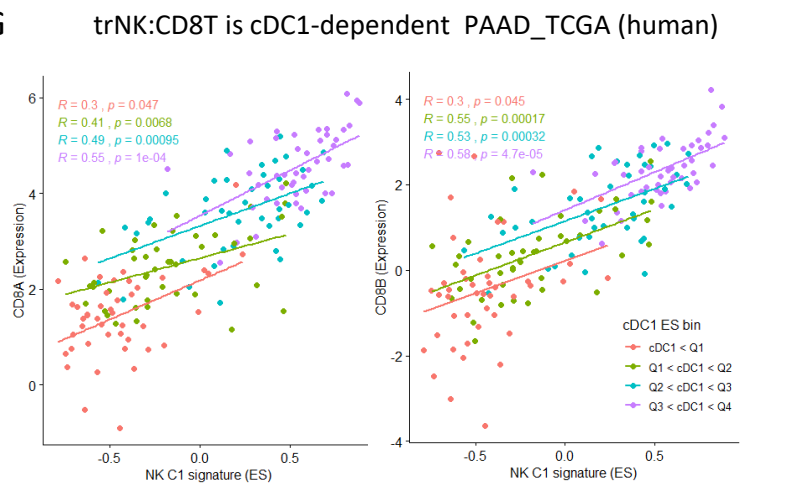
G
trNK:CD8T is cDC1-dependent PAAD_TCGA (human)
R = 0.3 , p = 0.047
R = 0.41 , p = 0.0068
R = 0.49 , p = 0.00095
R = 0.55 , p = 1e-04
R = 0.3 , p = 0.045
R = 0.55 , p = 0.00017
R = 0.53 , p = 0.00032
R = 0.58 , p = 4.7e-05
CD8A (Expression)
CD8B (Expression)
NK C1 signature (ES)
cDC1 ES bin
cDC1 < Q1
Q1 < cDC1 < Q2
Q2 < cDC1 < Q3
Q3 < cDC1 < Q4

Figure 7

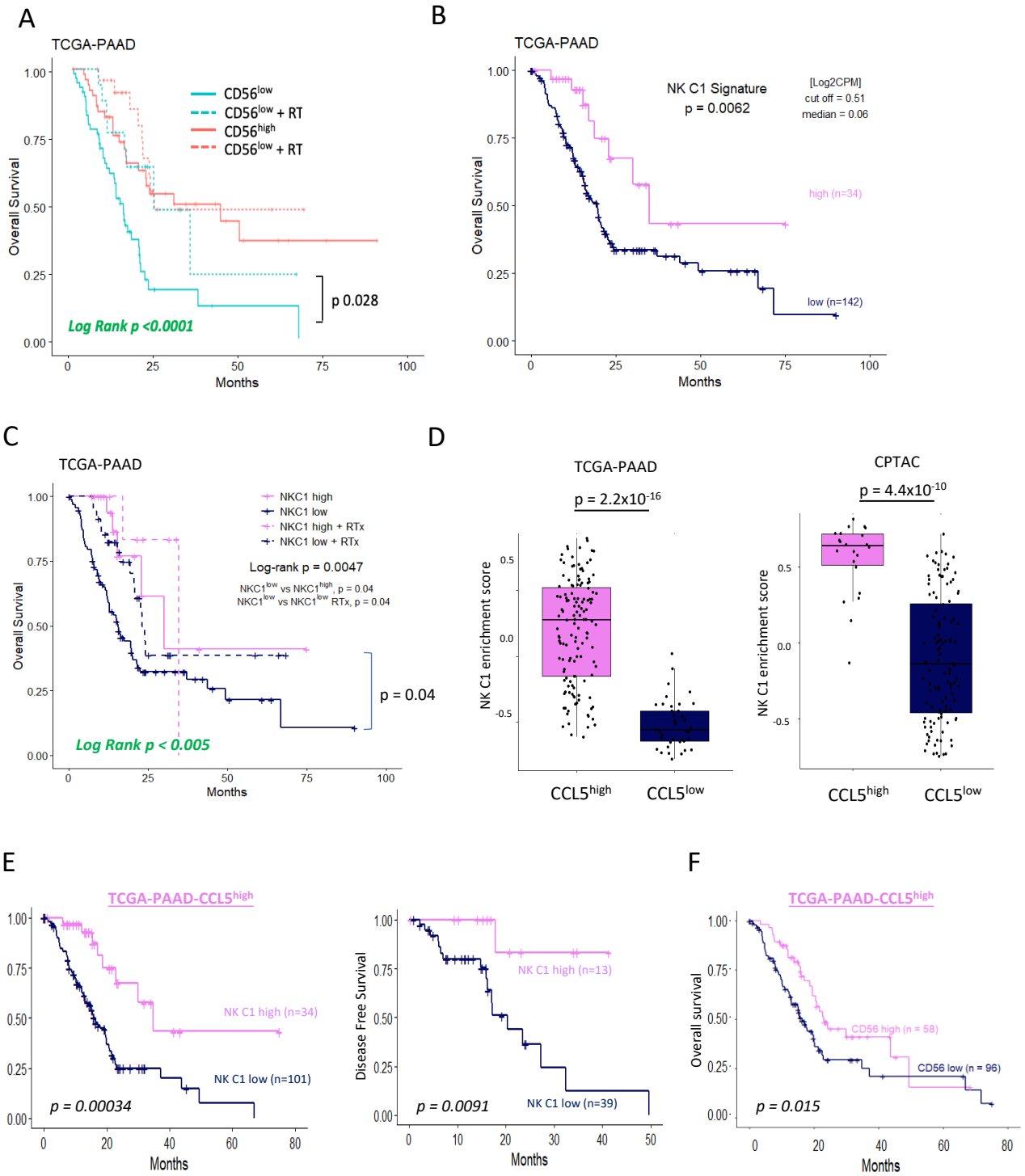
A
TCGA-PAAD
CD56low
CD56low + RT
CD56high
CD56low + RT
p 0.028
Log Rank p <0.0001
Overall Survival
Months
B
TCGA-PAAD
NK C1 Signature
p = 0.0062
[Log2CPM]
cut off = 0.51
median = 0.06
high (n=34)
low (n=142)
Overall Survival
Months
C
TCGA-PAAD
NKC1 high
NKC1 low
NKC1 high + RTx
NKC1 low + RTx
Log-rank p = 0.0047
NKC1low vs NKC1high, p = 0.04
NKC1low vs NKC1low RTx, p = 0.04
p = 0.04
Log Rank p < 0.005
Overall Survival
Months
D
TCGA-PAAD
p = 2.2x10-16
CPTAC
p = 4.4x10-10
NK C1 enrichment score
CCL5high
CCL5low
E
TCGA-PAAD-CCL5high
NK C1 high (n=34)
NK C1 low (n=101)
p = 0.00034
Overall survival
Months
NK C1 high (n=13)
NK C1 low (n=39)
p = 0.0091
Disease Free Survival
Months
F
TCGA-PAAD-CCL5high
CD56 high (n = 58)
CD56 low (n = 96)
p = 0.015
Overall survival
Months

Figure 8

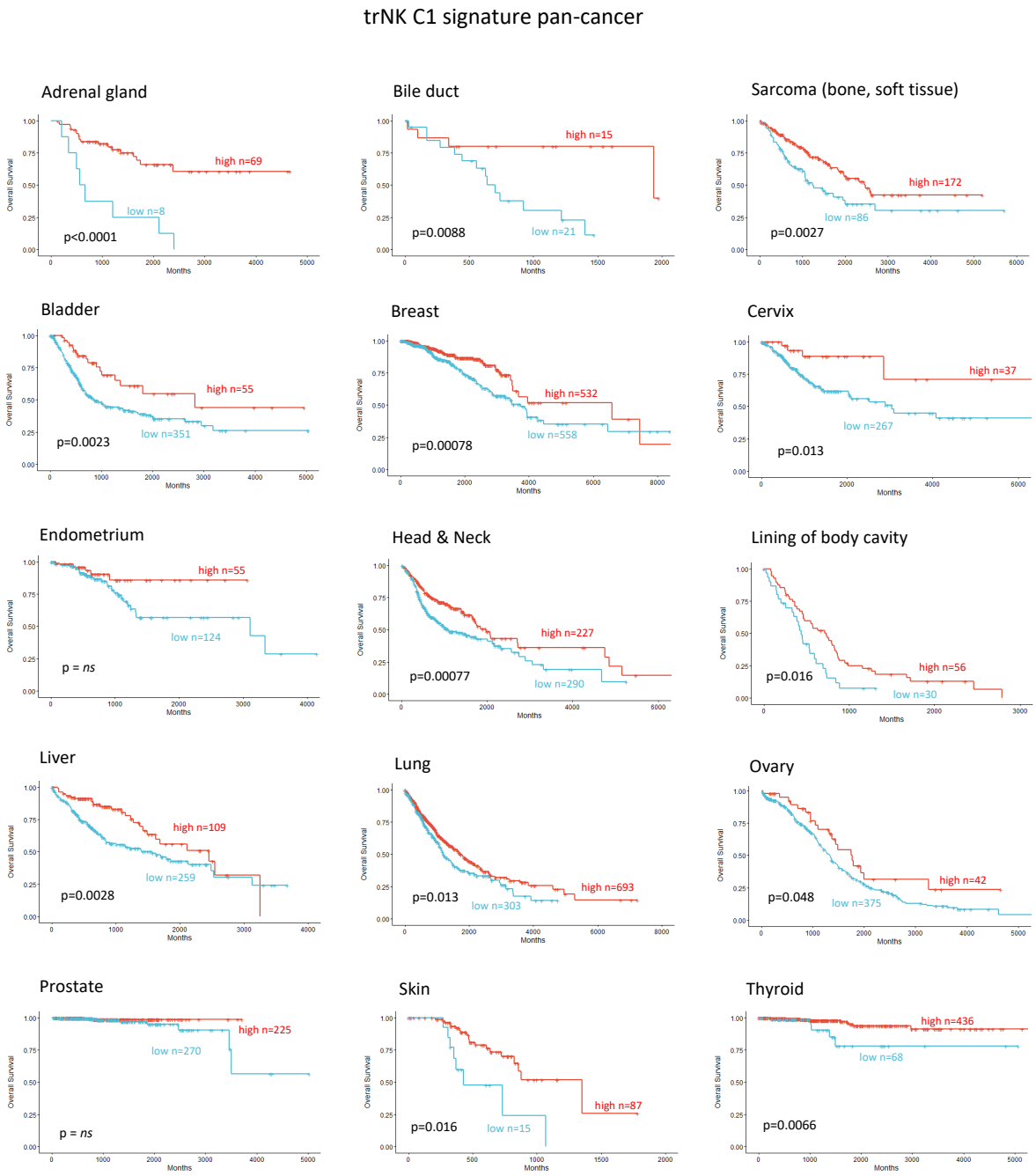
trNK C1 signature pan-cancer
Adrenal gland
high n=69
low n=8
p<0.0001
Bile duct
high n=15
low n=21
p=0.0088
Sarcoma (bone, soft tissue)
high n=172
low n=86
p=0.0027
Bladder
high n=55
low n=351
p=0.0023
Breast
high n=532
low n=558
p=0.00078
Cervix
high n=37
low n=267
p=0.013
Endometrium
high n=55
low n=124
p = ns
Head & Neck
high n=227
low n=290
p=0.00077
Lining of body cavity
high n=56
low n=30
p=0.016
Liver
high n=109
low n=259
p=0.0028
Lung
high n=693
low n=303
p=0.013
Ovary
high n=42
low n=375
p=0.048
Prostate
high n=225
low n=270
p = ns
Skin
high n=87
low n=15
p=0.016
Thyroid
high n=436
low n=68
p=0.0066
Overall Survival
Months